UNIVERSITY OF SOUTHAMPTON

FACULTY OF ENGINEERING SCIENCE AND MATHEMATICS

OPTOELECTRONICS RESEARCH CENTER

Suppression of Stimulated Brillouin Scattering in high power fibre lasers and amplifiers

by

Vladimir Hernandez-Solis

Thesis for the degree of Master of Philosophy

March 2009

UNIVERSITY OF SOUTHAMPTON

ABSTRACT

FACULTY OF ENGINEERING, SCIENCE & MATHEMATICS

OPTOELECTRONICS RESEARCH CENTER

Master of Philosophy

SUPPRESSION OF STIMULATED BRILLOUIN SCATTERING IN HIGH POWER FIBRE LASERS AND AMPLIFIERS

by Vladimir Hernandez-Solis

Fibre sources in high power devices have significant advantages over conventional gas and solid state lasers. However, for applications that require the so-called single-frequency sources with narrow linewidths, the output power is low mainly because of the problem of the stimulated Brillouin scattering (SBS).

A model that accounts for the SBS in dual-clad fibre lasers and amplifiers is presented. This was carried out in order to study the key parameters that affect the Brillouin threshold. Furthermore, the model was extended to account for the effect that the fibre axial temperature distribution has on the SBS threshold. Numerical solutions of the coupled differential equations for the evolution of the different beams showed a good agreement between the simulated data and reported experimental results. In addition, the model was used to study the relation of the core radius, the fibre length, and the fibre background loss on the SBS threshold. It was demonstrated that an adequate fibre structure design and a proper thermal management of the fibre amplifier lead to the supression of SBS.

Rare-earth doped fibre preforms with different compositions and geometries were fabricated by Modified Chemical Vapour Deposition technique in order to characterise the effect of doping and fibre structure on the Brillouin frequency and linewidth. Measurements using a microwave detection system for coherent detection of the anti-Stokes spontaneous Brillouin backscatter were performed on these fibres. The results showed that the actual Brillouin gain, linewidth and frequency shift widely differ from the values for pure fused silica fibres. It was confirmed that the fibre structure and composition play a big role in the Brillouin linewidth and Brillouin frequency shift of the fibre.

Contents

List of Figures

List of Tables

Declaration of Authorship

I, *Vladimir Hernandez-Solis*, declare that this thesis entitled

'Suppression of Stimulated Brillouin Scattering in high power fibre lasers and amplifiers',

and the work presented in the thesis are both my own, and have been generated by me as a result of my own original research. I confirm that:

- this work was done wholly or mainly while in candidature for a research degree at this University;
- where any part of this thesis has previously been submitted for a degree or any other qualification at this University or any other institution, this has been clearly stated;
- where I have consulted the published work of others, this is always clearly attributed;
- where I have quoted from the work of others, the source is always given. With the exception of such quotations, this thesis is entirely my own work;
- I have acknowledged all main sources of help;
- where the thesis is based on work done by myself jointly with others, I have made clear exactly what was done by others and what I have contributed myself;
- parts of this work have been published as: Refer to Appendix A (List of Publications).

Signed: ……..

Date:…….

Acknowledgements

First and foremost, I would like to express my sincere gratitude to my supervisor Dr. Jayanta Sahu for his invaluable advice , support and encouragement throughout my research. His valuable discussions contributed greatly to the accomplishment of this work.

I am also grateful to the postgraduate students and staff members of the Optoelectronics Research Centre who helped me with their discussions and feedback. These include Dr. Alexander Boyland, Dr. Mohammed Nasser Al Ahbabi, Dr. Trevor Newson, Prof. David Richardson, Dr. Johan Nilsson, and Dr. Eleanor Tarbox who assisted me in various capacities. Special thanks go to Eve Smith for her encouragement and follow up during all these years.

I acknowledge and wish to thank the National Council for Science and Technology in Mexico for the financial support I received to accomplish this research work.

I would like to thank my family, including my wife, parents and brother for their support, encouragement and patience.

This work is dedicated to the memory of Augusto.

Abbreviations

AOM	Acousto Optic Modulator
ASE	Amplified Stimulated Emission
BGS	Brillouin Gain Spectrum
BPF	Band Pass Filter
DFB	Distributed Feedback
EDFA	Erbium Doped Fibre Amplifier
ELO	Electrical Local Oscillator
EOM	Electro Optic Modulator
FUT	Fibre Under Test
FWHM	Full Width at Half Maximum
HPFA	High Power Fibre Amplifier
HPFL	High Power Fibre Laser
MCVD	Modified Chemical Vapour Deposition
MOPA	Master Oscillator Power Amplifier
NA	Numerical Aperture
OLO	Optical Local Oscillator
RE	Rare Earth
SBS	Stimulated Brillouin Scattering
SMF	Single Mode Fibre
YDFA	Ytterbium Doped Fibre Amplifier
YDFL	Ytterbium Doped Fibre Laser
YIG	Yttrium Iron Garnet

List of Symbols

A	Fibre core area
A_{eff}	Effective core area
$C_{\Delta\nu B}$	Brillouin linewidth temperature coefficient
$C\nu$	Brillouin frequency temperature coefficient
E1	Ground state level 1 in a four level laser system
E2	Energy level 2 in a four level laser system
E3	Energy level 3 in a four level laser system
E4	Energy level 4 in a four level laser system
g_B	Brillouin gain
$g_B(\nu)$	Brillouin Gain Spectrum
g_i	Amplifier gain induced by the RE-ions
g_p	Brillouin-gain peak value
g_{po}	Brillouin-gain peak value at room temperature
g_s	Seed signal gain induced by the RE-ions
g_{s1}	First order Stokes wave gain induced by the RE-ions
g_{s2}	Second order Stokes wave gain induced by the RE-ions
g_{s3}	Third order Stokes wave gain induced by the RE-ions
k	Conductivity of the fibre
L	Length of the amplifier
L_{eff}	Effective nonlinear interaction length
N_2	Fraction of ions in the meta-stable state
N_o	Density of the RE-dopant

P_n	Noise power from which SBS is initiated
P_p	Pump power
P_s	Seed signal power
P_{s1}	First order Stokes wave power
P_{s2}	Second order Stokes wave power
P_{s3}	Third order Stokes wave power
T(z)	Temperature as a function of the position along the fibre
Yb^{3+}	Ytterbium trivalen ion
z	Direction of propagation along the fiber
$\Delta T(z)$	Temperature difference between the origin and z
$\Delta\nu_B$	Brillouin linewidth; Full Width at Half Maximum
$\Delta\nu_{Bo}$	Brillouin linewidth at room temperature
Γ_i	Overlap of the guided mode with the dopant
α	Fibre backround loss
ν	Frequency
ν_B	Brillouin frequency shift
ν_{Bo}	Brillouin Frequency Shift at room temperature
ν_i	Frequency of the corresponding wave
σ_i^a	Absorption cross section from the ground state
σ_i^e	Emission cross section from the meta-stable state
τ_2	Upper-state lifetime

Chapter 1

1 Introduction

1.1 Introduction and Research Objectives

High-power devices such as high-power fibre-lasers (HPFL) and high-power fibre amplifiers (HPFA) have attracted much interest over recent years due to their numerous applications in various fields [1]-[6]. Fibre sources allow for simple thermal management, and offer single spatial mode, single polarization operation, and high efficiency, which are often difficult to achieve with conventional gas and solid state lasers. Recent reports of output powers over 1 kW from cladding-pumped ytterbium-doped (Yb^{3+}) fibre lasers (YDFLs) are impressive demonstrations of the power-scaling potential of cladding-pumped fibre lasers [6]-[10]. However, these lasers emit broad multi-frequency lines. For applications that require so-called single-frequency sources with narrow linewidths, of a few MHz or less, the output power on the other hand still remains significantly lower (a few hundreds of watts) mainly because of the problem of the stimulated Brillouin scattering (SBS).

SBS is a nonlinear process that occurs in optical fibres at optical intensities much lower than those needed for other nonlinear processes to take place. SBS threshold is reduced when the spectral width of the originating signal is narrower than the Brillouin linewidth, typically, 20 – 100 MHz in silica-based optical fibre; hence for single-frequency fibre-lasers or amplifiers SBS becomes the major limitation to achieving higher output powers [11]. Therefore, the comprehension of this

phenomenon is of utmost importance in order to increase its threshold in high power fibre devices.

The aim of this research into suppressing the stimulated Brillouin scattering present in high power devices is twofold. First, the objective is to identify the key parameters that affect the Brillouin frequency and linewidth; and second, to fabricate and characterise fibres that can be used in fibre amplifiers with an output power limited by the available pump power rather than by the SBS; i.e. to increase the SBS threshold to a value well above the signal output power achievable with the maximum available pump power.

It must be pointed out that the core of this research was done during the year 2004 and most of the results obtained were compared to publications on or before that year. A new literature review including the years since 2004 was performed and is included in this thesis.

1.2 Thesis Outline

Chapter two provides a detailed literature review and the background theory of this research work. HPFL's and HPFA's are decribed, their applications and major limitations are mentioned with emphasis given to the constraint that SBS represents in these devices. In this chapter the principles of SBS are also reviewed. An investigation of the parameters that affect the gain, linewidth and shift of this non linear phenomenon is also presented. Finally, the Modified Chemical Vapour Deposition (MCVD) technique for fibre fabrication along with the solution doping technique for rare-earth (RE) doping are described in detail.

Chapter three describes the work that has been carried out to numerically model the power in dual-clad fibre amplifiers including the effect of SBS. The SBS threshold is calculated by solving the differential equations for multiple orders of Stoke waves, pump and signal together with the rate equation for population inversion. This chapter also presents the results of the analysis performed on the parameters that affect the SBS threshold such as a temperature distribution along the fibre, and the fibre length, core radius, and background loss. Also, using the parameters from a

previously reported narrow-linewidth Master Oscillator Power Amplifier (MOPA) [12][13], it is concluded, in that particular experiment the temperature distribution along the fibre is the main reason the output power obtained experimentally was not limited by the presence of SBS but by the available pump power.

Chapter four includes the results of distributed Brillouin gain spectrum (BGS) measurements performed on fibres fabricated with different core geometries, dopants and doping concentrations. The method used to perform the measurements was a microwave detection system for coherent detection of the anti-Stokes spontaneous Brillouin backscatter. A brief description of the system set up and an overview of its principles of operation are presented.

Finally, chapter five provides conclusions to the research done and outlines possible future work.

Bibliography

[1] Hideur, T. Chartier, C. Özkul, F. Sanchez, “Dynamics and stabilization of a high power sided-pumped Yb-doped double-clad fiber laser,” Opt. Comm. 186, 311-317 (2000).

[2] M. Bashkansky, M.D. Duncan, L. Goldberg, J.P. Koplow, J. Reintjes, “Characteristics of a Yb-doped superfluorescent fiber source for use in optical coherence tomography,” Opt. Exp. 3(8), 305-310 (1998).

[3] S.V. Chernikov, J.R. Taylor, N.S. Platonov, V.P. Gapontsev, P.J. Nacher, G. Tastevin, M. Leduc, M.J. Barlow, “1083 nm ytterbium doped fiber amplifier for optical pumping of helium,” Electron. Lett. 33(9), 787-788 (1997).

[4] L. Goldberg, J.P. Koplow, R.P. Moeller, D.A.V. Kliner, “High power superfluorescent source with a sided-pumped Yb-doped double-cladding fiber,” Opt. Lett, 23(13), 1037-1039 (1998).

[5] M.J.F. Digonnet, Ed., Rare-Earth-Doped Fiber Lasers and Amplifiers, 2nd ed. (Marcel Dekker, Inc., New York, 1993).

[6] D.J. Richardson, Y. Jeong, C. Alegria, J.K. Sahu, R.B. Williams, A. Malinowski, A.N. Piper, J.H.V. Price, K. Furusawa, J. Nilsson, D.N. Payne, “The rising power of fibre laser technology,” EPS-QEOD Europhoton Conference Lausanne 29 Aug - 3 Sep 2004 Plenary Talk (Invited).

[7] Liem, J. Limpert, H. Zellmer, A. Tünnermann, V. Reichel, K. Mörl, S. Jetschke, S. Unger, H.-R. Müller, J. Kirchhof, T. Sandrok, A. Harschak, “1.3 kW Yb-doped fiber laser with excellent beam quality,” in OSA Trends in Optics and Photonics Series (TOPS) Vol. 96, Conference on Lasers and Electro-Optics (CLEO), Technical Digest, Postconference Edition (Optical Society of America, Washington, DC 2004), paper CPDD2 (2004).

[8] Y. Jeong, J.K. Sahu, S. Baek, C. Alegria, C.A. Codemard, D.B.S. Soh, V. Philippov, D.J. Richardson, D.N. Payne, J. Nilsson, "Ytterbium-doped double-clad large-core fiber lasers with kW-level continuous-wave output power," CLEO/IQEC and PhAST Technical Digest on CD-ROM (The Optical Society of America, Washington, DC 2004), paper CMS1 (2004).

[9] Y. Jeong, J.K. Sahu, S. Baek, C. Alegria, C.A. Codemard, D.B.S. Soh, V. Philippov, R.B. Williams, K. Furusawa, D.J. Richardson, D.N. Payne, J. Nilsson, "The rising power of fibre lasers," in IEEE/LEOS 2003 Arizona26-30 Oct. 2003 (invited).

[10] D.N. Payne, Y. Jeong, J. Nilsson, J.K. Sahu, D.B.S. Soh, C. Alegria, P. Dupriez, C.A. Codemard, V.N. Philippov, V. Hernandez, R. Horley, L. Hickey, L. Wanzcyk, C.E. Chryssou, J.A. Alvarez-Chavez, P.W. Turner, "Kilowatt-class single-frequency fiber sources," in Proc. SPIE 5709, 133-141 (2005).

[11] Liem, J. Limpert, H. Zellmer, A. Tünnermann, "100-W single-frequency master-oscillator fiber power amplifier," Opt. Lett. 28(17), 1537-1539 (2003).

[12] Y. Jeong, J. Nilsson, J.K. Sahu, D.B.S. Soh, C.A. Alegria, P. Dupriez, C.A. Codemard, D.N. Payne, R. Horley, L.M.B. Hickey, L. Wanzcyk, C. Chryssou, J.A. Alvarez-Chavez, P.W. Turner, "Single-frequency, single-mode, single-polarization ytterbium-doped fiber MOPA source with 264 W of continuous-wave output power," in OSA Trends in Optics and Photonics Series (TOPS) Vol. 96, Conference on Lasers and Electro-Optics (CLEO), Technical Digest, Postconference Edition (Optical Society of America, Washington, DC 2004), paper CPDD1 (2004).

[13] Y. Jeong, J. Nilsson, J.K. Sahu, D.B.S. Soh, C.A. Alegria, P. Dupriez, C.A. Codemard, D.N. Payne, R. Horley, L.M.B. Hickey, L. Wanzcyk, C. Chryssou, J.A. Alvarez-Chavez, P.W. Turner, "Single-frequency, single-mode, plane-polarized ytterbium-doped fiber master oscillator power amplifier source with 264 W of output power," Opt. Lett. 30(5), 459-461 (2005).

Chapter 2

2 Literature Review and Theoretical Background

2.1 Introduction

This chapter outlines the theory behind high power fibre lasers and amplifiers with particular emphasis being given to the limitation that stimulated Brillouin scattering imposses on the output power. A literature review highlights the main characteristics of these devices and the recent achievements regarding power increase. Brillouin scattering and the factors that affect the frequency shift, gain, and linewidth of this non linear phenomenon are reviewed. Finally, a description of the Modified Chemical Vapour Deposition together with the solution doping technique used to manufacture the fibres used for this research is provided.

2.2 High Power Fibre Lasers and Amplifiers

2.2.1 Introduction

High power fibre lasers and amplifiers are very attractive devices because of their numerous applications in various domains. The fibre geometry in these devices grants a high surface to volume ratio and a beneficial waveguide effect [1]. The

former allows for simple thermal management while the latter avoids thermo-optical problems under significant heating conditions [1]. This technology also offers single spatial mode, single polarization operation, high efficiency and excellent beam quality [2][3][4], all of which are often difficult to achieve with conventional gas and solid state lasers.

Ongoing continuous research on these type of lasers and amplifiers has led to increasing output powers in these systems. During the past few years, powers greater than 1 kW achieved with cladding-pumped ytterbium-doped (Yb^{3+}) fibre lasers have been reported in a number of references [5]-[10]. These lasers emit broad multi-frequency lines, either restricted by the wide gain spectrum, or by the bandwidth of a wavelength selective filter. Typically, the linewidth in these devices is in the order of tens of nanometers [11]. These systems are suitable in applications, such as materials processing or industrial solutions, where only high power and good beam quality are desired and the broad linewidth does not represent a problem [11].

On the other hand, applications such as coherent beam combination, gravitational wave detection, differential absorption lidar, resonant fluorescent spectroscopy, and nonlinear frequency conversion, require single-frequency fibre sources with narrow linewidths of a few MHz or less [11]-[14]. Primarily limited by the stimulated Brillouin scattering, the power in these fibre lasers and amplifiers still remains low compared with the broad linewidth systems [11][13][15]-[19].

2.2.2 Double-clad Fibres

Clearly, the output power in fibre lasers depends on the amount of power used to pump the system. In fibre lasers and amplifiers, their small size presents a limitation on the amount of power that can be used. High pump power results in high power density in the core resulting in facet damage and lower thresholds for non linear phenomena such as SBS. Therefore, cladding pumping and large area cores are preferable.

In general, high power fibre lasers and amplifiers are achieved with rare-earth doped double-clad fibres. In a double-clad fibre, a RE-doped core is enclosed by a lower refractive index inner cladding which, in turn, is surrounded by an even lower index outer cladding. Simple-clad fibres have a very low injection efficiency for large

stripe laser diodes [20], whereas the double-clad geometry facilitates the side [17] or end pumping by high-power laser diodes, resulting in a high launching efficiency due to the multimode pump propagation through the inner cladding. The modes of the inner cladding overlap with the core and thus the pump power can be absorbed there [4]. The propagation of the laser wavelength takes place only throughout the single-mode core. In order for the modes in the inner cladding to overlap with the core, and thus increase the absorption of the pump, the axial symmetry of the fibre has to be broken, for instance by making flats on the fibre or by having an offcentre core.

As mentioned before, high power carries the problem of high power density in the fibre core. Moreover, a large ratio of cladding to core area results in weak pump absorption and thus longer fibres are needed to increase the interaction length [21][22]. Therefore, it is desirable to have a large core area in order to reduce the power density and increase the pump absorption. On the other hand, large cores result in a larger number of supported modes hence affecting the single mode output [21]. It is well known however, that higher order modes are much more affected by bend losses than lower order modes [21][23]. Hence, high single mode output powers can still be obtained from large cores by bending or coiling the fibre [21][24].

2.2.3 Fibre Length and Doping Concentration

In HPFL's and HPFA's, the fibre length depends on the RE-doping concentration. The length has to be such that the maximum amount of pump power is absorbed. Thus the higher the doping concentration the higher the gain and the shorter the fibre. On the other hand, due to the fact that high-power is confined within the core, nonlinear effects such as stimulated Brillouin scattering or Raman scattering are favoured; therefore, a shorter fibre is preferred since the effective nonlinear interaction length is reduced and hence the nonlinear power threshold is increased. However, the doping level is limited to the point where concentration clustering due to interionic energy transfer occurs [25]. Therefore a delicate balance between the fibre length and the fibre doping concentration has to be achieved when designing fibres for high power fibre devices.

2.2.4 Principles of Operation

In nature, atoms interact with photons by absorption or emission of the latter resulting in upward and downward transitions between the atom energy levels. Because of energy conservation, the energy of the photon will be equal to the difference between the energy levels where the transition took place. When a photon is emitted from an atom, it can be due to either spontaneous or stimulated emission. While spontaneous emission depends only on the transition cross-section and not on the amount of photons in the mode, stimulated emission requires a photon to interact with the atom and stimulate the emission of another photon of the same energy, polarisation and direction as the incident photon. As previously stated, the energy of the atomic transitions has to be the same as that of the photons, therefore, only a small band of frequencies can be amplified. For instance, ytterbium is a rare-earth metal widely used as a dopant in the fibre laser technology in the form of a trivalent ion (Yb^{3+}) with the energy level $^2F_{5/2}$ for the excited state with three sub-levels, and $^2F_{7/2}$ for the ground state with four sub-levels (see Figure 2.1).

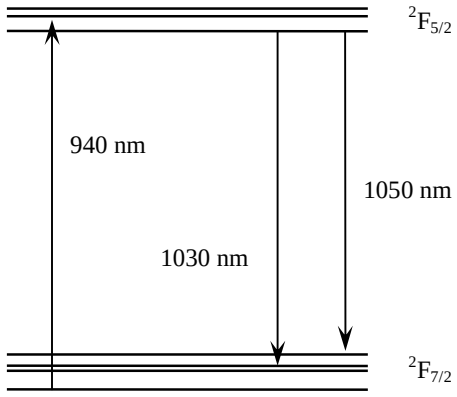

Figure 2.1: *Energy band diagrams for Yb^{+3} ions in Yb:YAG, and the usual pump and laser transitions. After [1].*

Figure 2.2 shows the spectral dependence on the cross sections in ytterbium doped silica similar to the one used for fibre lasers. It can be observed that at 915 nm there is a broad range for pumping while at 975 nm the higher absorption level occurs in a narrow range. On the other hand, there is a high emission peak at 975 nm and a broad emission spectrum around 1060 nm [1]. Due to the fact that the ions are used within a molecule, the energy levels are broadened, as observed in Figure 2.2, thus increasing the amplifier's operating bandwidth.

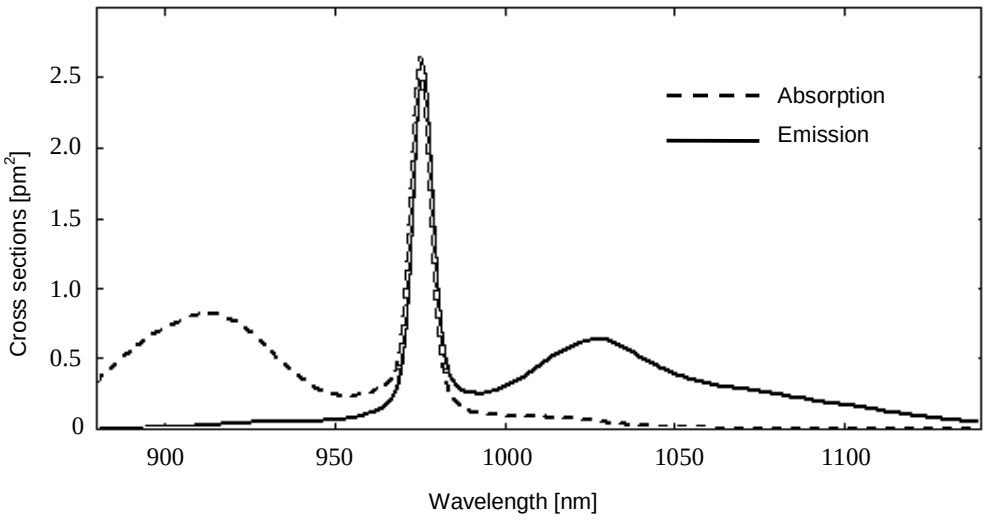

Figure 2.2: *Emission and absorption cross-sections as a function of the wavelength in ytterbium doped germanosilicate glass. After [1].*

Amplification will only occur when a population inversion is present in the medium, i.e., there are more atoms in the excited state than in the ground state, otherwise the light will be absorbed rather than used to stimulate emission. Since different energy levels have different time decay values or lives, population inversion can be achieved by choosing the correct energy levels and the appropriate pumping rate. For example, in a four level laser system, like the one shown in Figure 2.3, the pump will excite the atoms from the ground state to the excited energy level 4 (E4). There is a very fast transition into the energy level 3 (E3) and, eventually, the atoms will decay from E3 to the energy level 2 (E2). However, E3 has a much longer life time than E2, and thus, with the appropriate pumping rate, the amount of excited atoms in level E3 will exceed that of level E2 hence achieving population inversion. The difference between E3 and E2 is the laser transition. When the atoms in E2 deplete to the ground state E1, the process will repeat.

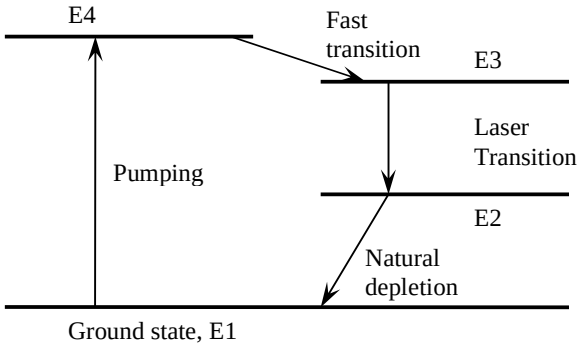

Figure 2.3: *Four level laser system diagram.*

A signal at the lasing energy transition can be seeded and amplified if the pump rate is sufficient to maintain the population inversion.

Optical oscillators can be used, together with the amplification principle explained above, in order to achieve a laser. Regarding fibre lasers and amplifiers, the gain medium can be the doped fibre and the cavity can be formed by means of mirrors or Bragg gratings. As long as the round trip in the cavity is formed by an integer number of wavelengths (phase condition) and the small signal gain is greater than the cavity loss (gain condition) lasing will occur.

High power fibre amplifiers can be modelled by a set of differential equations for the pump, seed and rate equation for population inversion. A model, including the effect Brillouin scattering has on an amplifier that is seeded with a narrow linewidth signal, will be developed and explained in Chapter 3.

2.3 Stimulated Brillouin Scattering

In optical fibres SBS originates when the optical field corresponding to the forward travelling narrow-linewidth signal, interferes with photons scattered in the backward direction off thermally excited acoustic phonons. This process generates an acoustic wave through the process of electrostriction, which in turn induces a travelling Bragg grating. Increasing the signal power increases the strength of this grating, and above threshold, there is a rapid growth in the power of the backscattered travelling wave. The backward wave, referred to as a Stokes wave, is generated at a Brillouin frequency (ν_B), which in turn is equivalent to the Doppler shift of the narrow-line signal determined by the velocity of sound in the medium. SBS is characterized by the Brillouin gain spectrum peaking at ν_B.

Assuming that the acoustic waves decay exponentially, the BGS at room temperature presents a Lorentzian shape of the form [26]

$$g_B(\nu) = g_p \frac{\left(\Delta\nu_B/2\right)^2}{(\nu-\nu_B)^2 + \left(\Delta\nu_B/2\right)^2} = \left(g_p \Delta\nu_B\right) \frac{\Delta\nu_B}{4(\nu-\nu_B)^2 + (\Delta\nu_B)^2} \qquad (2.1)$$

where $\Delta\nu_B$ is the full width at half maximum of the BGS, and g_p is the Brillouin-gain peak value that takes place at the Brillouin frequency $\nu=\nu_B$. The product between the Brillouin-gain peak value and the Brillouin linewidth ($g_p\Delta\nu_B$) is always constant and is temperature independent [27].

In the case of polarization maintaining optical fibres, the Brillouin gain coefficient for pure fused silica is 5×10^{-11} mW^{-1}[26]. This value is dependent upon physical characteristics of the medium such as the longitudinal elasto-optic coefficient. Thus, different dopants, or their concentration, affect the effective Brillouin gain peak value.

Shiraki, Ohashi and Tateda [28] showed that the SBS threshold is very dependent upon the frequency shift distribution along the fibre. Therefore, in order to reduce the amount of SBS, techniques to change the frequency shift distribution have to be studied and applied.

Also, variations on the geometry or composition along the fibre that affect the acoustic wave propagation, and thus change the Brillouin frequency and the Brillouin linewidth, must lead to a reduction in the amount of SBS. A changing core geometry along the fibre such as a tapered core or a nonuniform doping distribution help to suppress the SBS.

The dependence of both the Brillouin frequency and Brillouin linewidth on the fibre composition, strain, temperature, and geometry has been widely studied [27]-[41]. Shiraki [35] and Yu, et al. [34], have shown that the Brillouin frequency shift is a function of the core radius. Moreover, the larger the core area the lower the power density and thus the nonlinear thresholds increase. On the other hand, Ohashi and Tateda [38] showed that applying a nonuniform dopant concentration over a strain-free fibre, would lead to an increase in the SBS power threshold of up to 17 dB. Nikles et al. [27] illustrated that high doping concentration in GeO_2 doped fibres yielded a broad Brillouin linewidth and thus a high SBS threshold. Hence it is desirable to have high doping concentrations to reduce the amount of SBS in the fibre.

Regarding the strain in the fibre, Yoshizawa and Imai [39] demonstrated that an increase of up to 9 dB in the SBS threshold is possible by applying a sinusoidal strain distribution along the fibre. Furthermore, Yoshizawa, Horiguchi, and Kurashima

[40] showed that the Brillouin linewidth can increase up to 2.9 times with cyclic strain. It must be pointed out that features such as stress sections in polarization maintaining fibres also apply a certain degree of strain and may lead to a reduction in the effective Brillouin gain [42].

Concerning the temperature distribution along the fibre, it has been widely studied and shown in conventional passive fibres used for telecommunications, that it modifies the frequency shift distribution along the fibre and even the Brillouin linewidth [27]-[33]. Therefore, in fibre amplifiers where a temperature distribution is present along the fibre, the corresponding backscattered power will be reduced.

2.3.1 Effect of SBS in Single Frequency Narrow Linewidth HPFLs

As of now, the output power in narrow linewidth single frequency high power fibre lasers and amplifiers still remains significantly lower compared with that of their broad linewidth counterparts (a few hundreds of watts). The nonlinear effect of stimulated Brillouin scattering can limit the performance when the laser linewidth is narrower than the Brillouin bandwidth of typically 20 – 100 MHz in silica-based optical fibre. The backscattered optical and acoustic waves product of the SBS reduce the output power. This is known to become the major limitation in achieving higher output powers in high power fibre devices [11][13][15]-[19]. Moreover, when the SBS threshold is reached, the backscattered power can arrive at levels that are dangerous to the pump and seed.

However, a single-frequency, single-mode, plane-polarized ytterbium-doped fibre master-oscillator power amplifier (MOPA) with 264 W output power, not limited by the SBS but by the available pump power, was reported by Jeong, et al. [43] [44]. It is reported that the final-stage amplifier operated with a gain of 19 dB and a conversion efficiency of 68%, and no evidence of any significant backscattered power was observed. The lack of SBS was mainly attributed to the temperature distribution in the fibre. This MOPA result, will be used as a reference in subsequent chapters in order to prove the validity of the amplifier's analytical model that accounts for the effect of SBS.

2.4 Modified Chemical Vapour Deposition (MCVD)

Due to its simplicity and flexibility, MCVD has become one of the major fabrication processes of high-quality glass fibre lightguides for applications such as optical communications and fibre lasers and amplifiers. Moreover, complex refractive index profiles can be achieved by means of MCVD. This was the technique employed to manufacture some of the fibres used in this research.

In essence, high-purity material is deposited on the inner surface of a high-quality pure fused silica tube. The deposited material combines with the silica forming a glass whose refractive index is different from that of pure silica according to the type of material. Successive layers are deposited to form the desired cladding/core structure. Afterwards, the tube is collapsed to form a rod with the required configuration for light guidance. The refractive index profile and relative geometry of the preform are preserved when it is drawn into fibre.

The initial high-quality pure fused silica tube is chosen according to the desired final geometry. It is cleaned and then carefully mounted, aligned and straightened in a lathe so that it rotates concentrically. A traversing oxyhydrogen torch is used as a source for heating the tube to temperatures above 2,000 °C [45]. One of the ends of the tube is connected through a rotating leak-tight joint to a system that delivers chemicals in the form of gasses of controlled pressure. The other end, will serve as the exit of the system; it is connected to a larger tube (in diameter) that in turn is fixed to a chemical scrubbing system. This larger tube serves as a collector for the material that is not incorporated.

The first step is to polish the tube in order to shrink existing bubbles and eliminate, or at least smooth out, any surface irregularities.

Subsequently, chemicals are injected through the entrance of the tube in the form of a gas stream. This is performed by passing oxygen through highly pure halide compounds in bubblers [46]. The halide-oxygen mix is then injected in the same direction as the traversing torch is heating up the rotating tube. The heat induced by the torch causes the halides to react with the oxygen producing oxides, in the form of glassy particles, and forming Cl_2 as a by-product. The particles are deposited and fused to form a glassy film (up to 100µm thick) down-stream of the hot zone [45].

The process is repeated and multiple layers are used to tailor the desired index profile. Usually, the first layers are pure silica forming a cladding layer of low OH silica to avoid diffusion of OH from the original tube into the core. The type of gas used depends upon the cladding or core's desired composition. GeO_2 is the most common dopant used to increase the refractive index. The dopant source for GeO_2 is $GeCl_4$ [46]. Fluorine is used for compositions where the refractive index is desired to be below that of the pure silica [45]. The fluorine incorporation is mainly dependent on the concentration of SiF_4 in the gas stream.

Next, the tube is collapsed to a solid rod at very high temperatures. This step usually takes most of the preform processing time and is critical to achieve the desired dimensions of the final fibre. Collapse is carried out by heating the tube to temperatures above 2,000 °C, thus reducing the tube diameter [47]. Many successive and slow passes are performed.

As explained in section 2.2.2, breaking the axial symmetry of the fibres or having off-centre cores help the modes traveling in the inner cladding of a double-clad fibre amplifier to overlap with the core resulting in more pump absorption and shorter fibre lengths. This involves machining the preform. For instance, a flat can be milled on the side of the preform in order to break axial symmetry. On the other hand, birefrigent fibres can be achieved by drilling holes in the preform and inserting stress rods in the holes; the induced stress and the holes will create asymmetry in perpendicular directions resulting in a birefrigent fibre. Moreover, it has been demonstrated that induced stress during manufacturing can help in reducing the amount of SBS in fibres [42].

2.4.1 Solution Doping

Due to the low vapour pressure of the inorganic RE-compounds, it is extremely difficult to use vaporisation for delivering the chemicals. Therefore, a solution doping technique has to be used in order to incorporate RE-ions in the preform.

The MCVD process is undertaken until the layer which will contain the rare earth ions is to be deposited. The oxide soot is deposited using a temperature between 1,400 and 1,800 °C which is not high enough to consolidate the silica particles but is

sufficient to make the $SiCl_4$ react with oxygen in order to provide SiO_2 [48]. This leads to a porous silica layer where the rare earths can be accommodated.

A solution of a RE-compound is prepared using a rare earth chloride dissolved in methanol. The tube is removed from the lathe and the solution is pumped into it. After about an hour [48], the solution is drained slowly and the tube is left in the lathe to dry. The next step is to consolidate the soot layer by heating the tube until the soot layer has sintered into glass. This step is performed under an O_2 rich environment to oxidise the compounds and remove oxidised solvent molecules.

Once the core is finished, the MCVD process is completed to collapse the tube.

2.4.2 Fibre drawing

Once the preform is produced by the MCVD process, or any other fibre fabrication method, it is drawn to achieve the desired optical fibre diameter. The preform is accurately placed in a graphite furnace that works in an argon environment free of oxygene to avoid oxidation. A glass weight (silica drop) attached to the bottom of the preform provides enough tension to pull it down. Above 1900 °C the drop stretches and pulls down the preform, when the glass is around 1mm thick the drop is cut off and the glass is pulled by hand until it reaches the capstan. Once attached to the capstan, the automatic process starts. Mass conservation law plays an important role in fibre drawing, the fibre diameter goes down at the feeding to drawing velocities ratio. Closed loop control mechanisms allow for accurate fibre diameter control.

Drawing temperatures vary from 1950 °C and 2250 °C [45]. Temperature is critical in order to keep the right viscosity of the glass and thus avoid fibre breakage and reduce optical losses. It is well known that higher temperatures result in higher losses [45]. The temperature and the drawing velocity determine the tension in the pulling process. It has been found that 30 g is the optimum tension to minimise the optical loss in the fibre [45]. However, fibre lasers and amplifiers have special shapes (e.g. flat sides or holey fibres) and at the optimum pulling tension the preform will tend to become circular because of the low viscosity. Therefore, the fibres used for these devices have to be drawn at a relatively low temperature.

Coatings can be applied at the end of the pulling process. The fibre will pass through coating material that is usually cured by ultraviolet light or by thermal curing. This will improve the mechanical properties of the fibre and reduce the probability of breakage. Moreover, in a cladding pumped fibre system, the coating will have a refractive index lower than that of the silica cladding, which provides the silica cladding with a waveguide characteristic for the pump beam.

Bibliography

[1] Paschotta, R., Encyclopedia of Laser Physics and Technology, (Wiley-VCH, Weinheim, Germany, 2008).

[2] M.J.F. Digonnet, Ed., Rare-Earth-Doped Fiber Lasers and Amplifiers, 2nd ed. (Marcel Dekker, Inc., New York, 1993).

[3] E. Desuivre, Erbium-Doped Fiber Amplifiers Principles and Applications, (Wiley, New York, 2002).

[4] R. Paschotta, J. Nilsson, A.C. Tropper, D.C. Hanna, "Ytterbium-Doped Fiber Amplifiers," IEEE J. of Quantum Electron. 33(7), 1049-1056 (1997).

[5] D.J. Richardson, Y. Jeong, C. Alegria, J.K. Sahu, R.B. Williams, A. Malinowski, A.N. Piper, J.H.V. Price, K. Furusawa, J. Nilsson, D.N. Payne, "The rising power of fibre laser technology," EPS-QEOD Europhoton Conference Lausanne 29 Aug - 3 Sep 2004 Plenary Talk (Invited).

[6] Liem, J. Limpert, H. Zellmer, A. Tünnermann, V. Reichel, K. Mörl, S. Jetschke, S. Unger, H.-R. Müller, J. Kirchhof, T. Sandrok, A. Harschak, "1.3 kW Yb-doped fiber laser with excellent beam quality," in OSA Trends in Optics and Photonics Series (TOPS) Vol. 96, Conference on Lasers and Electro-Optics (CLEO), Technical Digest, Postconference Edition (Optical Society of America, Washington, DC 2004), paper CPDD2 (2004).

[7] Y. Jeong, J.K. Sahu, S. Baek, C. Alegria, C.A. Codemard, D.B.S. Soh, V. Philippov, D.J. Richardson, D.N. Payne, J. Nilsson, "Ytterbium-doped double-clad large-core fiber lasers with kW-level continuous-wave output power," CLEO/IQEC and PhAST Technical Digest on CD-ROM (The Optical Society of America, Washington, DC 2004), paper CMS1 (2004).

[8] Y. Jeong, J.K. Sahu, D.N. Payne, J. Nilsson, "Ytterbium-doped large-core fiber laser with 1.36 kW continuous-wave output power," Opt. Exp. 12, 6088-6092 (2004).

[9] V. Reichel, K.W. Moerl, S. Unger, S. Jetschke, H.R. Mueller, J. Kirchof, T. Sandrock, A. Harschack, A. Liem, J. Limpert, H. Zellmer, A. Tunnermann, "Fiber-laser power scaling beyond the 1-kilowatt level by Nd:Yb co-doping," in Proceedings SPIE 5777, 404-407 (2005).

[10] Y. Jeong, J.K. Sahu, S. Baek, C. Alegria, C.A. Codemard, D.B.S. Soh, V. Philippov, R.B. Williams, K. Furusawa, D.J. Richardson, D.N. Payne, J. Nilsson, "The rising power of fibre lasers," in IEEE/LEOS 2003 Arizona26-30 Oct. 2003 (invited).

[11] S. Gray, D. Walton, J. Wang, A. Liu, M. Li, X. Chen, A. Ruffin, J. DeMeritt, and L. Zenteno, "Suppression of Stimulated Brillouin Scattering in High Power, Narrow Linewidth Fiber Amplifiers," in Nonlinear Optics: Materials, Fundamentals and Applications, OSA Technical Digest (CD) (Optical Society of America, 2007), paper WB2.

[12] M. Wickham, J. Anderegg, S. Brosnan, D. Hammons, H. Komine, M. Weber, "Coherently coupled high power fiber arrays," in Proc. Advanced Solid State Photonics, Santa Fe, NM, USA, Feb. 1-4, 2004, paper MA4.

[13] M. Mermelstein, A. Yablon, and C. Headley, "Suppression of Stimulated Brillouin Scattering in an Er-Yb Fiber Amplifier Utilizing Temperature-Segmentation," in Optical Amplifiers and Their Applications, Technical Digest (CD) (Optical Society of America, 2005), paper TuD3.

[14] P. Dragic, C. Liu, G. Papen, and A. Galvanauskas, "Optical Fiber with an Acoustic Guiding Layer for Stimulated Brillouin Scattering Suppression," in Conference on Lasers and Electro-Optics/Quantum Electronics and Laser Science and Photonic Applications Systems Technologies, Technical Digest (CD) (Optical Society of America, 2005), paper CThZ3.

[15] Liem, J. Limpert, H. Zellmer, A. Tünnermann, "100-W single-frequency master-oscillator fiber power amplifier," Opt. Lett. 28(17), 1537-1539 (2003).

[16] V.I. Kovalev, R.G. Harrison, J. Nilsson, Y. Jeong, V. Hernandez-Solis, J.K. Sahu, "Analytic modeling of Brillouin gain in rare-earth doped fiber amplifiers with high-power single-frequency signals," in Fiber Lasers Technology, Systems and Applications II, Proceedings SPIE, 2005, 5709, paper 23.

[17] L. Zenteno, "High-Power Double-Clad Fiber Lasers," J. Lightwave Technol. 11(9), 1435-1446 (1996).

[18] D.N. Payne, Y. Jeong, J. Nilsson, J.K. Sahu, D.B.S. Soh, C. Alegria, P. Dupriez, C.A. Codemard, V.N. Philippov, V. Hernandez, R. Horley, L. Hickey, L. Wanzcyk, C.E. Chryssou, J.A. Alvarez-Chavez, P.W. Turner, "Kilowatt-class single-frequency fiber sources," in Proc. SPIE 5709, 133-141 (2005).

[19] Y. Jeong, J. Nilsson, J.K. Sahu, D.N. Payne, R. Horley, L.M.B. Hickey, and P.W. Turner, "Power Scaling of Single-Frequency Ytterbium-Doped Fiber Master-Oscillator Power-Amplifier Sources up to 500 W," IEEE J. of Sel. Top. on Quantum Electron. 13(3), 546-551 (2007).

[20] Hideur, T. Chartier, C. Özkul, F. Sanchez, "Dynamics and stabilization of a high power side-pumped Yb-doped double-clad fiber laser," Opt. Comm. 186, 311-317 (2000).

[21] J.P. Koplow, Dahv A. V. Kliner, and Lew Goldberg, "Single-mode operation of a coiled multimode fiber amplifier," Opt. Lett. 25, 442-444 (2000).

[22] N. G. R. Broderick, H. L. Offerhaus, D. J. Richardson, R. A. Sammut, J. Caplen, and L. Dong, "Large mode area fibers for high power applications," Opt. Fiber Tech. 5,185 (1999).

[23] C.D. Poole, S.C. Wang, "Bend-induced loss for the higher-order spatial mode in a dual-mode fiber," Opt. Lett. 18(20), 1712-1714 (1993).

[24] J. M. Fini, "Bend-compensated design of large-mode-area fibers", Opt. Lett. 31 (13), 1963 (2006).

[25] F. Auzel, P. Goldner, "Towards rare-earth clustering control in doped glasses," Opt. Mat. 16(1-2), 93-103 (2001).

[26] Agrawal, G.P., Nonlinear Fiber Optics, 3rd ed. (Academic Press, San Diego, CA, 2001).

[27] M. Nikles, L. Thevenaz, P.A. Robert, "Brillouin Gain Spectrum Characterization in Single-Mode Optical Fibers," J. Lightwave Technol. 15(10), 1842-1851 (1997).

[28] K. Shiraki, M. Ohashi, M. Tateda, "SBS Threshold of a Fiber with a Brillouin Frequency Shift Distribution," J. Lightwave Technol. 14(1), 50-57 (1996).

[29] S. Le Flohic, P. Cambon, "Study of Brillouin gain spectrum in standard single-mode optical fiber at low temperatures (1.4-370 K) and high hydrostatic pressures (1-250 bars)," Opt. Comm. 219, 395-410 (2003).

[30] J. Hansryd, F. Dross, M. Westlund, P.A. Andrekson, S.N. Knudsen, "Increase of the SBS Threshold in a Short Highly Nonlinear Fiber by Applying a Temperature Distribution," J. Lightwave Technol. 19(11), 1691-1697 (2001).

[31] T. Kurashima, T. Horiguchi, M. Tateda, "Thermal Effects of Brillouin Gain Spectra in Single-Mode Fibers," IEEE Photon. Technol. Lett. 2(10), 718-720 (1990).

[32] Q. Yu, X. Bao, L. Chen, "Temperature dependence of Brillouin frequency, power, and bandwidth in panda, bow-tie, and tiger polarization-maintaining fibers," Opt. Lett. 29(1), 17-19 (2004).

[33] Y. Imai, N. Shimada, "Dependence of Stimulated Brillouin Scattering on Temperature Distribution in Polarization-Maintaining Fibers," IEEE Photon. Technol. Lett. 5(11), 1335-1337 (1993).

[34] J.W. Yu, Y. Park, K. Oh, I.B. Kwon, "Brillouin frequency shifts in silica optical fiber with the double cladding structure," Opt. Exp. 10(19), 996-1002 (2002).

[35] K. Shiraki, M. Ohashi, M. Tateda, "Suppression of stimulated Brillouin scattering in a fibre by changing the core radius," Electron. Lett. 31(8), 668-669 (1995).

[36] J. Botineau, E. Picholle, D. Bahloul, "Effective stimulated Brillouin gain in singlemode optical fibres," Elect. Lett. 31(23), 2032-2034 (1995).

[37] N. Shibata, R.G. Waarts, R.P. Braum, "Brillouin-gain spectra for single-mode fibers having pure-silica, GeO2-doped, and P2O5-doped cores," Opt. Lett. 12(4), 269-271 (1987).

[38] M. Ohashi, M. Tateda, "Design of Strain-Free-Fiber with Nonuniform Dopant Concentration for Stimulated Brillouin Scattering Suppression," J. Lightwave Technol. 11(12), 1941-1945 (1993).

[39] N. Yoshizawa, T. Imai, "Stimulated Brillouin Scattering Suppression by Means of Applying Strain Distribution to Fiber with Cabling," J. Lightwave Technol. 11(10), 1518-1522 (1993).

[40] N. Yoshizawa, T. Horiguchi, T. Kurashima, "Proposal for Stimulated Brillouin Scattering Suppression by Fibre Cabling," Electron. Lett. 27(12), 1100-1101 (1991).

[41] X.P. Mao, R. W. Tkach, A.R. Chraplyvy, R.M. Jopson, R.M. Derosier, "Stimulated Brillouin Threshold Dependence on Fiber Type and Uniformity," IEEE Photon. Tehnol. Lett. 4(1), 66-69 (1992).

[42] Y. Hibino, T. Edahiro, T. Horiguchi, Y. Azuma, N. Shibata, "Evaluation of residual stress and viscosity in SiO2-core/F-SiO2 clad single-mode optical fibers from Brillouin gain spectra," J. Appl. Phys. 66(9), 4049-4052 (1989).

[43] Y. Jeong, J. Nilsson, J.K. Sahu, D.B.S. Soh, C.A. Alegria, P. Dupriez, C.A. Codemard, D.N. Payne, R. Horley, L.M.B. Hickey, L. Wanzcyk, C. Chryssou, J.A. Alvarez-Chavez, P.W. Turner, "Single-frequency, single-mode, single-polarization ytterbium-doped fiber MOPA source with 264 W of continuous-wave output power," in OSA Trends in Optics and Photonics Series (TOPS) Vol. 96, Conference on Lasers and Electro-Optics (CLEO), Technical Digest, Postconference Edition (Optical Society of America, Washington, DC 2004), paper CPDD1 (2004).

[44] Y. Jeong, J. Nilsson, J.K. Sahu, D.B.S. Soh, C.A. Alegria, P. Dupriez, C.A. Codemard, D.N. Payne, R. Horley, L.M.B. Hickey, L. Wanzcyk, C. Chryssou, J.A. Alvarez-Chavez, P.W. Turner, "Single-frequency, single-mode, plane-polarized ytterbium-doped fiber master oscillator power amplifier source with 264 W of output power," Opt. Lett. 30(5), 459-461 (2005).

[45] T. Li, Optical Fiber Communications, Volume 1 Fiber Fabrication, (Academic Press, Orlando, Florida 1995).

[46] J.B. MacChesney, P.B. O'Connor. 1995. MCVD method for making a low OH Fiber Preform with a Hydrogen-free heat source. U.S. Patent 5,397,372, filed November 30, 1993, and issued March 14, 1995.

[47] F.P. Partus, G.A. Thomas. 1982. Optical Fiber Fabrication. U.S. Patent 4,334,903, filed February 1, 1980, and issued June 15, 1982.

[48] J. E. Townsend, S. B. Poole, D. N. Payne, "Solution-doping technique for fabrication of rare earth doped optical fibres," Electron. Lett. 23(7), 329-331 (1987).

Chapter 3

3 Fibre Amplifier Analytical Model Including the Effect of SBS

3.1 Introduction

A model to describe the evolution of the different waves (pump, seeded signal, and different order Stokes powers) that propagate along the fibre amplifier under steady-state conditions was implemented. The model follows closely those by dos Santos Ferreira [1] and Brilliant [2]. It was considered that the rare-earth doped amplifier has been seeded with a narrow-line single-frequency signal at one end of the fibre, while the RE-ions were optically pumped through the other end of the fibre. The pump beam has a broad bandwidth so it does not cause any SBS. However, the signal linewidth is narrower than the Brillouin-gain spectrum, and can generate a Brillouin Stokes wave. This is also narrow-band, and can generate higher order Stokes waves. The amplifier can be modelled as a system of differential equations for the pump, signal, Stokes power, and population inversion. The technique used to solve the set of differential equations was the shooting method for two boundary value problems combined with a globally convergent Newton-Raphson algorithm.

The model was used to simulate the propagation of the power waves along a fibre amplifier, accounting for the effect of SBS in a variety of fibre designs. This was done in order to study the effect that the fibre physical characteristics, such as length,

core radius, and doping concentration, have on the SBS threshold. Moreover, equations for the effect that a temperature distribution along the fibre has on the SBS threshold were developed. The model shows that a temperature distribution along the fibre results in higher SBS thresholds. The modelled data agree well with previously reported experimental results [3].

3.2 Analytical Model

A fibre amplifier can be modelled as a system of differential equations for the pump, signal, and Stokes powers. Under steady-state conditions, the set of differential equations that describes the evolution of the pump (P_p), the narrow-line signal (P_s), and the first, second and third-order Stokes (P_{s1}, P_{s2}, P_{s3} respectively) along the amplifier, can be written as [1][4]

$$\frac{dP_p}{dz} = -(g_p - \alpha)P_p \tag{3.1}$$

$$\frac{dP_s}{dz} = -\frac{g_B}{A_{eff}}(P_{s1} + P_n)P_s + (g_s - \alpha)P_s \tag{3.2}$$

$$\frac{dP_{s1}}{dz} = -\frac{g_B}{A_{eff}}(P_{s1} + P_n)P_s + \frac{g_B}{A_{eff}}(P_{s2} + P_n)(P_{s1} + P_n) - (g_{s1} - \alpha)P_{s1} \tag{3.3}$$

$$\frac{dP_{s2}}{dz} = \frac{g_B}{A_{eff}}(P_{s2} + P_n)(P_{s1} + P_n) - \frac{g_B}{A_{eff}}(P_{s3} + P_n)(P_{s2} + P_n) + (g_{s2} - \alpha)P_{s2} \tag{3.4}$$

$$\frac{dP_{s3}}{dz} = -\frac{g_B}{A_{eff}}(P_{s3} + P_n)(P_{s2} + P_n) - (g_{s3} - \alpha)P_{s3} \tag{3.5}$$

where A_{eff} is the effective core area, α is the fibre background loss, P_n is the input noise power from which SBS is initiated, g_B is the Brillouin-gain coefficient, and g_i is the amplifier gain induced by the RE-ions. The amplifier gain is given by [2] [5]

$$g_i = \pm\left[\left(\sigma_i^e + \sigma_i^a\right)N_2 - \sigma_i^a\right]N_o\Gamma_i \tag{3.6}$$

where σ_i^a and σ_i^e are the absorption and emission cross-sections, from the ground state and the meta-stable upper state respectively, N_o is the density of the RE-dopant

ions in the core, Γ_i is the mode overlap of the guided mode with the dopant, and N_2 is the fraction of ions in the meta-stable level. The subscript *i*, indicates the corresponding propagating wave. In the steady-state, the normalized inversion can be written as [2] [5]

$$N_2 = \frac{\sum_i \frac{\sigma_i^a \Gamma_i P_i}{Ah\nu_i}}{\frac{1}{\tau_2} + \sum_i \frac{(\sigma_i^e + \sigma_i^a)\Gamma_i P_i}{Ah\nu_i}} \tag{3.7}$$

where τ_2 is the upper-state lifetime, ν_i is the frequency of the corresponding wave, and *A* is the fibre core area.

It was assumed that only one excited meta-stable state and the ground state were populated. Furthermore, the seeding of the Stokes wave by spontaneous emission from the RE-ions, as well as amplification of broadband spontaneous emission by the RE-ions, have been neglected. This is justified if the RE-induced gain is too small for ASE to reach high power, and the spontaneous emission within the bandwidth of the Stokes waves is small compared to the spontaneous Brillouin scattering.

3.3 Constants and parameters used in the model

Unless specified, the fibre geometry, background loss and the doping characteristics for the model are those published by Y. Jeong, et al. in reference [3]. The Master Oscillator Power Amplifier used in [3] is illustrated in Figure 3.1.

Figure 3.1 shows a plane polarized Distributed Feedback (DFB) fibre laser working at 1060 nm with an output power of 80 mW followed by four Ytterbium Doped Fibre Amplifers (YDFA). The first three YDFA's are made of standard non-Polarization Mantaining fibres used as intermediate stages. The DFB laser was narrow-linewidth with a linewidth below 60 kHz.

The final amplifier was made of a 6.5 m long double-clad fibre. It had a 25 μm diameter core with an NA below 0.06. The inner cladding was 380 μm in diameter with a nominal NA of 0.48. The fibre had two borosilicate stress rods, resulting in a core birefringence of ~2×10^{-4}. The pump was launched into the signal output end

from a 975 nm diode source. The available pump power was 390 W. The Yb^{3+} concentration was around ~6500 ppm by weight resulting in a small signal cladding absorption coefficient of ~2 dB/m at 975 nm. The maximum ouput power at 1060 nm was 264 W and was limited by the available pump power. No sign of SBS was observed even at the maximum pump power. The slope efficiency, with respect to the launched pump power, was 72%.

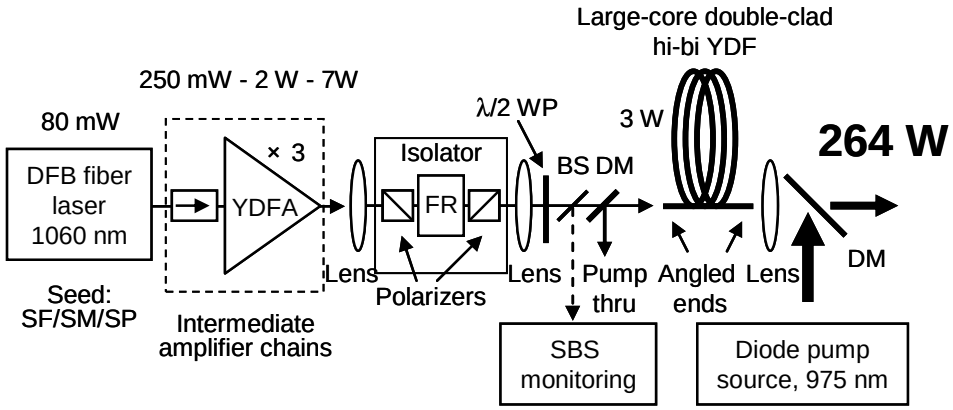

Figure 3.1: *Experimental set-up for the YDFA used as a reference for the analytical model presented in this work; DM: dichroic mirror; BS: beam splitter; FR: Faraday rotator; WP: waveplate; SF/SM/SP: single-frequency/single-mode/single-polarization. After [3].*

For calculations where no temperature effects are accounted for, the effective Brillouin-gain coefficient used along the fibre was $g_{B\text{-}eff}=5\times10^{-11}$ mW^{-1} . The value used for the input noise power was 0.5 nW [1]. For the ytterbium, both the absorption and emission cross-sections were taken as $25x10^{-25}$ m^2 [6][7] at 975 nm, whereas at 1060 nm, which is the amplified wavelength, the absorption cross-section used was 0.03×10^{-25} m^2, and the emission cross-section used was 3×10^{-25} m^2 [6][7]. The upper-state ($^2F_{5/2}$) lifetime of Yb was taken as 0.84 ms [7].

3.6 Simulation Results

Figure 3.2 shows the simulation results for the fibre parameters as described above. In this case, no temperature effect was considered. At $z = L$, where L is the length of the amplifier, the pump power and the counter-propagating first-order Stokes waves were taken as 390 W and 0.5 nW respectively, whereas at $z = 0$, the input signal power is equal to 3 W [3]. These are the known boundary conditions at both ends of the amplifier. Equations (3.1)-(3.3) were solved in MATLAB® using the shooting method for two-point boundary value problems together with a globally convergent Newton-Raphson algorithm.

The output power obtained was 111 W, i.e. the amplifier gain was only around 16 dB. On the other hand, the total gain observed for the first-order Stokes was 111 dB. Equation (3.3) shows that the gain experienced by the first-order Stokes is a combination of the amplifier gain and the Brillouin gain. The Brillouin gain will be equal to the total gain of the first-order Stokes minus the gain of the amplifier. Therefore, the Brillouin gain observed was ~95 dB. Moreover, the second and third order Stokes waves present ~100 dB and ~70 dB gains respectively.

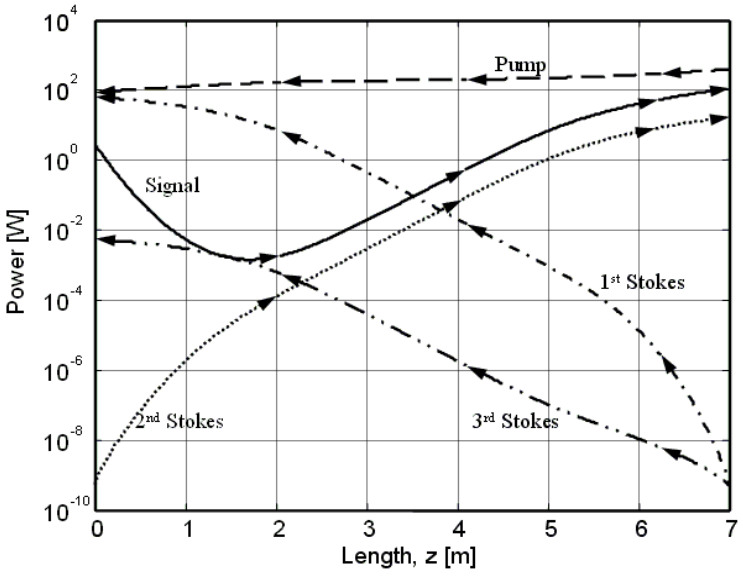

Figure 3.2: *Modelled data that depict the evolution of the signal power, pump power, and first to third order Stokes powers along the amplifier used in [3]. The temperature effect is not taken into account. The arrow-heads show the propagation direction.*

Figure 3.2 shows poor agreement with the experimental results reported in [3]. In the experiment, the absence of SBS was tentatively attributed to thermal effects which were not taken into account for the simulation shown in Figure 3.2. This will be investigated in the next section.

3.4 Effect of a temperature distribution along the fibre

It is well documented that the Brillouin frequency shift and the Brillouin linewidth depend on the temperature in the fibre [8]-[13]. Thus, when there is a temperature gradient along the fibre, the SBS gain should be reduced and the SBS threshold power must increase [9]. The model was improved to account for the temperature distribution along the fibre length. The modelled data showed that the effective Brillouin linewidth for the whole fibre is broadened and the effective Brillouin-gain is reduced well below its room temperature value.

The total Brillouin frequency shift at any point along the fibre can be obtained by adding the shift contribution to the Brillouin frequency shift at the beginning of the fibre caused by the temperature differential. The fibre is assumed to be at room temperature. Hence, the Brillouin frequency shift can be expressed as

$$\nu_B(z) = \nu_{B_o} + C_\nu[T(z) - T(0)] = \nu_{B_o} + C_\nu \Delta T(z) \tag{3.8}$$

where ν_{Bo} is the Brillouin frequency shift at room temperature, C_ν is the Brillouin frequency temperature coefficient in HzK^{-1}, $T(z)$ is the temperature as a function of the position along the fibre, and $\Delta T(z)$ is the temperature difference between the beginning and any point located at a position equal to z along the fibre.

Furthermore, the Brillouin linewidth will also be different at any point along the fibre. It can be written as

$$\Delta\nu_B(z) = \Delta\nu_{B_o} + C_{\Delta\nu B}[T(z) - T(0)] = \Delta\nu_{Bo} + C_{\Delta\nu B}\Delta T(z) \tag{3.9}$$

where $\Delta\nu_{Bo}$ is the Brillouin linewidth at room temperature, and $C_{\Delta\nu B}$ is the Brillouin linewidth temperature coefficient in HzK^{-1}.

Since the Brillouin linewidth and the Brillouin frequency are affected when a temperature distribution is present at any point along the fibre, equation (2.1) can be rearranged by substituting equations (3.8) and (3.9), and the Brillouin-gain coefficient can be rewritten as a frequency and position dependent function as

$$g_B(\nu,z)=\left(g_{p_o}\Delta\nu_{B_o}\right)\frac{\Delta\nu_{B_o}+C_{\Delta\nu B}\Delta T(z)}{4\left(\nu-\nu_{B_o}-C_\nu\Delta T(z)\right)^2+\left(\Delta\nu_{B_o}+C_{\Delta\nu B}\Delta T(z)\right)^2} \qquad (3.10)$$

where g_{po} is the Brillouin-gain peak value at room temperature that takes place at $\nu=\nu_{Bo}$.

The effective BGS can be obtained by averaging the individual contribution of the Brillouin-gain spectra at any position along the fibre, i.e.

$$g_B(\nu)=\frac{1}{L}\int_0^L g_B(\nu,z)dz \qquad (3.11)$$

Concerning the evaluation of the temperature difference, the heat generated will be mainly due to the quantum efficiency of the amplifier, background absorption and scattering, and nonradiative transition and decay [14]. From the perspective of energy conservation, the heat dissipated per unit volume in the fibre will be proportional to the difference between the input and the output optical powers flowing in through a unit of volume at a given position in the fibre [14]. Therefore, if the heat dissipation is uniform along the length of the fibre, and the heat transfer along the *z* direction is assumed to be due to conduction, the temperature difference can be expressed as

$$\sum_i P_i^{\pm}(z)+\sum_i P_i^{\pm}(0)=k\Delta T(z) \qquad (3.12)$$

where the upper index indicates direction of propagation, i.e. indicates whether the power of the corresponding beam flows into or out of the unit of volume, hence it has to be added or subtracted accordingly. The constant *k* corresponds to the conductivity of the fibre.

Equation (3.10) describes the Brillouin-gain coefficient at any point along the fibre length when a temperature distribution according to equation (3.12) is present, and can be used in equations (3.2)-(3.5) in order to find the evolution of the different powers along the amplifier.

3.4.1 Simulation Results Accounting for a Temperature Distribution Along the Fibre

The simulations were based on the fibre characteristics and pumping scheme depicted in [3]. In the experiment, when the pump power was 390 W the output signal was 264 W, and $\Delta T(L)$ was estimated to be 100 K. The temperature value was obtained solving the Poisson equation for the temperature distribution in the fibre based on the pump absorption rate [14][15]. The input values for $C_{\Delta\nu B}$ and C_{ν} were taken as -0.23 $MHzK^{-1}$ and 1.7 $MHzK^{-1}$ respectively. Even though these parameters are dependent upon the wavelength and fibre characteristics, the assumed values are typical [11]. The Brillouin-gain bandwidth used was 36 MHz [11], and the Brillouin frequency 11 GHz [15]. The results are plotted in Figure 3.3. A signal output power of 264 W was obtained with the input signal of 3 W. The amplifier gain was 19 dB, and the Brillouin gain observed is around 53 dB; this fitted well to the experimental results. It can also be observed that the second and third order Stokes waves present a significantly smaller gain (~19 dB and ~18 dB respectively) compared to that obtained by the model that does not account for the temperature distribution along the fibre (~100 dB and ~70 dB respectively).

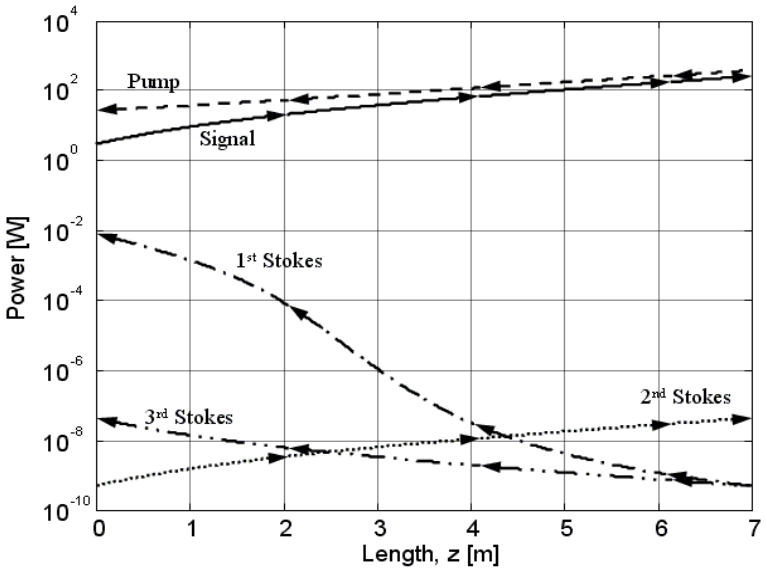

Figure 3.3: *Modelled data that depict the evolution of the signal power, pump power, and first to third order Stokes powers along the fibre. The temperature effect has been taken into consideration. The arrow-heads show the propagation direction.*

According to [3], SBS was negligible and hence it could not be recorded. However, the simulations showed that even though the amplifier output power remained essentially unaffected by the presence of the weak first order Stokes, some SBS could have been recorded during the experiment. This is due to the fact that the peak Brillouin-gain coefficient at room temperature considered was 5×10^{-11} mW^{-1}. This value corresponds to pure fused silica. It has been reported, [13][16][17][18] that the Brillouin-gain coefficient and the Brillouin linewidth are widely dependent on both the dopant and its concentration, and also on stress in the fibre [13][19][20]. Since the fibre used in the experiment [3] was highly doped with ytterbium and contained a pair of borosilicate stress rods for polarized output, the actual SBS gain coefficient may well be lower than the assumed one. Even a relatively modest decrease of the Brillouin gain would reduce the SBS power calculated with the model, and this would be in closer agreement with the experiment.

Figure 3.4 shows the signal output power as a function of the pump power for cases when the temperature effect is considered and when it is not. The slope efficiency for the temperature inclusive case is 70%, which is in close agreement with the reported experimental results of 72% [3]. It is thus clear that the text-book Brillouin-gain coefficient value of 5×10^{-11} mW^{-1} for cases where no temperature effect is accounted for, exaggerates the actual Brillouin gain value, and hence the results plotted in Figure 3.2 differ significantly from those obtained experimentally.

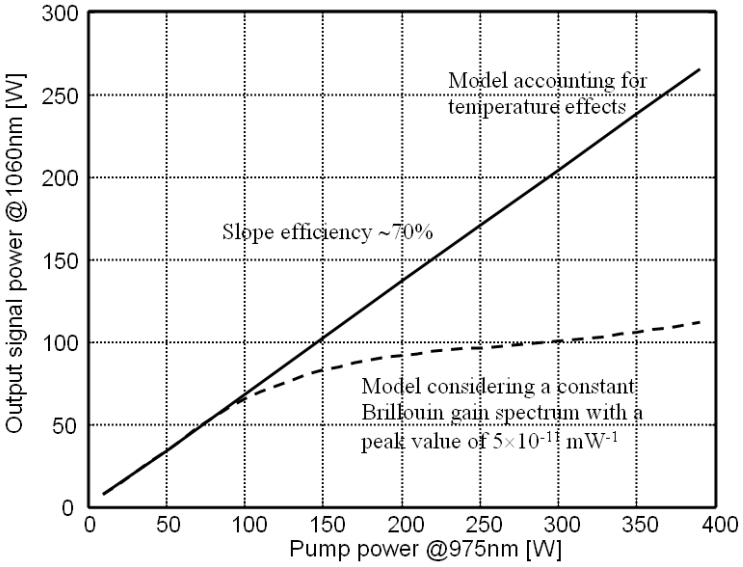

Figure 3.4: *Signal output power as a function of the pump power for both models, the one accounting for the temperature and the constant Brillouin-gain model.*

Figure 3.5 shows the temperature distribution along the amplifier calculated using equation (3.12). To obtain the power value of the traveling waves in the amplifier it was assumed to have negligible SBS, a pump power equal to 390 W, and an output power of 264 W.

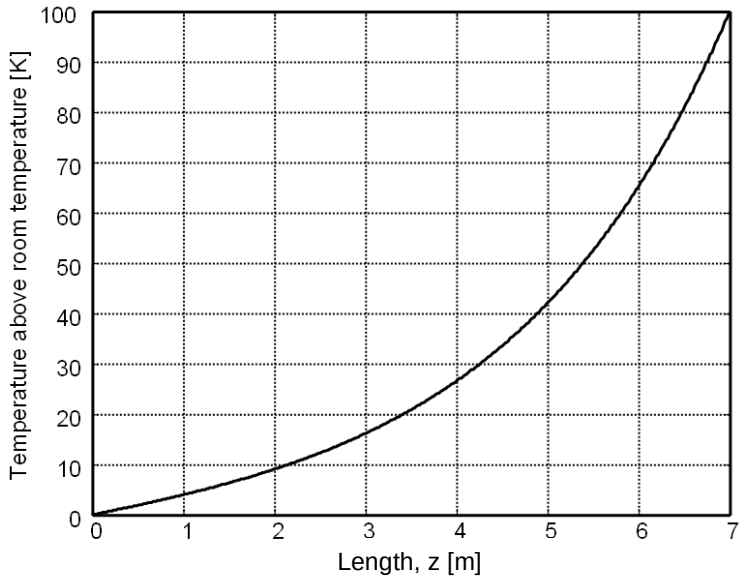

Figure 3.5: *Temperature distribution along the fiber when the pump power is equal to 390 W and the signal output power is equal to 264 W. Calculated using equation (3.12).*

Figure 3.6 shows the BGS for a silica fibre at room temperature together with the BGS for the same fibre under the temperature distribution shown in Figure 3.5. The Brillouin-gain peak value for the whole fibre is reduced to more than half its value at room temperature thus explaining the lack of SBS observed during the experiment. Furthermore, the peak value is shifted from 11 GHz to 11.015 GHz and the Brillouin linewidth increased from 36 MHz at room temperature to 82 MHz for the calculated temperature distribution.

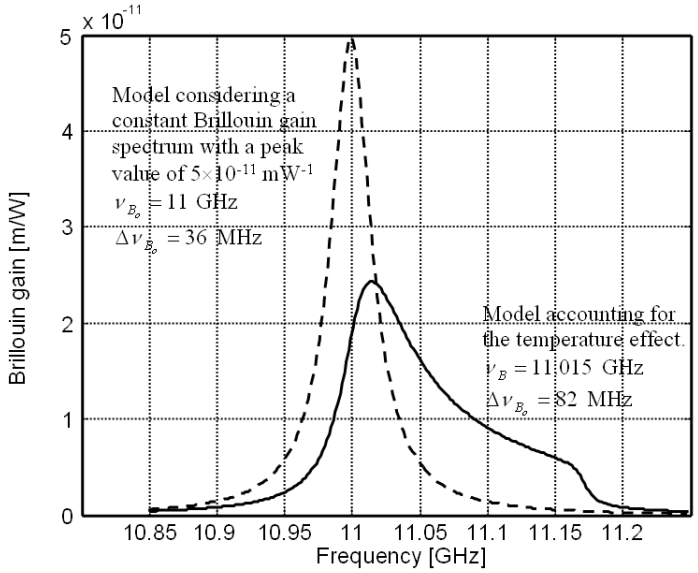

Figure 3.6: *BGS for a silica fibre at room temperature and for the same fibre under the calculated temperature distribution.*

In Figure 3.7, the first order Stokes is plotted against the signal output power. When the temperature distribution shown in Figure 3.5 was not taken into account, the SBS threshold was reached at a very low output power (~55 W), and the Stokes power builds rapidly. Conversely, when the temperature effect was taken into consideration, the SBS was negligible, its threshold was not reached even at the highest output power and, thus, the output power was only limited by the available pump power.

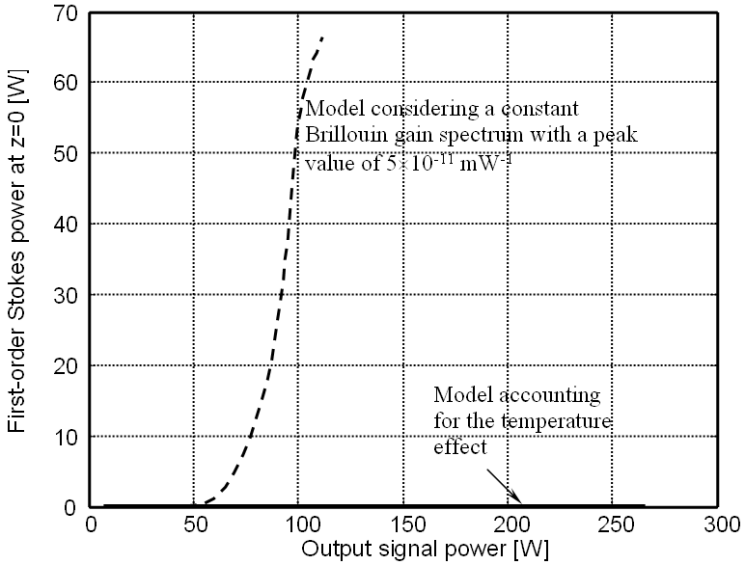

Figure 3.7: *First order Stokes power at the beginning of the fiber (z=0) as a function of the signal output power for both models, the one accounting for the temperature distribution shown in Figure 3.5 and the constant Brillouin gain model.*

3.5 Dependence of SBS on the fibre length, core radius and background loss

Physical characteristics of the fibre such as the fibre composition, core radius, fibre length, and fibre background loss, are key parameters that affect the SBS threshold. Using the implemented model, this section shows the SBS dependence on these fibre parameters.

3.5.1 Dependence of SBS on the fibre length

It is clear that longer fibres should have a lower SBS threshold because of the longer effective length of interaction for the nonlinear process to take place. Figure 3.8 shows the first order Stokes power at the beginning of the fibre as a function of the amplifier output power for different fibre lengths. Note that the longer the fibre length the sooner the SBS power begins to increase rapidly, i.e. long fibres present a lower SBS threshold. The inset in Figure 3.8 shows the trend of the SBS power threshold as a function of the fibre length.

The fabrication of short fibres, in order to reduce the SBS in the system, limits the amplifier performance because less pump power will be absorbed, this can be observed in Figure 3.9. In the case of a 5 m long fibre, SBS never affects the amplifier performance in the pump-range shown; the output power never becomes depleted and the amplifier shows a slope efficiency (between the pump and the output powers) of 61%. Conversely, for a 9 m long fibre the amplification process is affected by the SBS when the output goes above 250 W; however, the slope efficiency at lower pump powers is 73% which is greater compared to that shown by the 5 m amplifier.

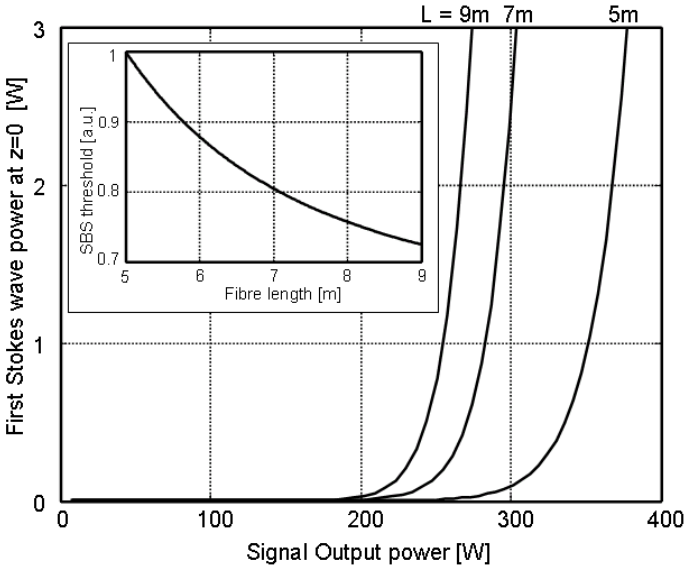

Figure 3.8: *First order Stokes power at the beginning of the fibre (z=0) as a function of the signal output power for different fibre lengths. The trend that the SBS threshold has as a function of the fibre length is shown in the inset.*

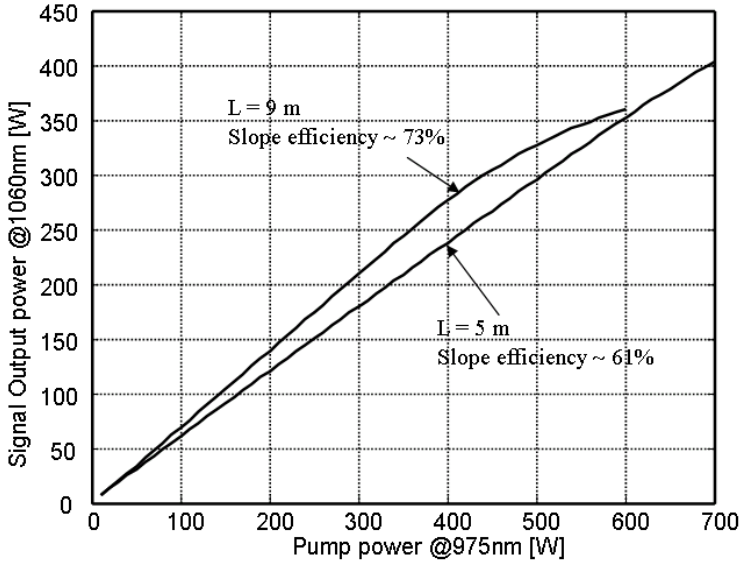

Figure 3.9: *Signal output power as a function of the pump power for different fibre lengths.*

3.5.2 Dependence of SBS on the fibre background loss

As for the background loss, in equations (3.1) – (3.5) it is assumed that there is a similar loss for the pump, signal, and Stokes powers with a loss coefficient α. The amount of the backscattered Stokes power is mainly governed by the amount of signal power along the amplifier length. However, equation (3.13) [21] shows that the effective length of Brillouin interaction is reduced as the background loss increases, hence a higher SBS threshold is expected for fibres with a high background loss.

$$L_{eff} = \left[1 - \exp(-\alpha L)\right] / \alpha \tag{3.13}$$

In equation (3.13), L_{eff} is the effective nonlinear interaction length, L is the length of the fibre, and α is the fibre background loss.

Figure 3.10 shows the optimum length, i.e. the one at which the maximum output power was achieved with a pump power equal to 390 W, as a function of the background loss. For a background loss greater than 0.4 dB/m, the fibre length decreases as the background loss increases. Conversely, for a background loss smaller than 0.4 dB/m, the optimum length increases as the background loss increases. This can be attributed to the fact that for small values of background loss, the amount of pump power absorbed leads to a signal power above the SBS threshold. In this region, the optimization process suggests that it is better to have shorter fibres for smaller values of background loss so that less interaction length is available for the nonlinear process to take place. On the other hand, above a certain background loss value, the amount of pump power absorbed is not sufficient to generate inconvenient values of Stokes power, i.e. SBS is negligible to the amplifier performance. Therefore, above a certain value of background loss, for a fixed pump power, SBS becomes insignificant, and the optimization process indicates to have shorter fibres in order to avoid higher losses.

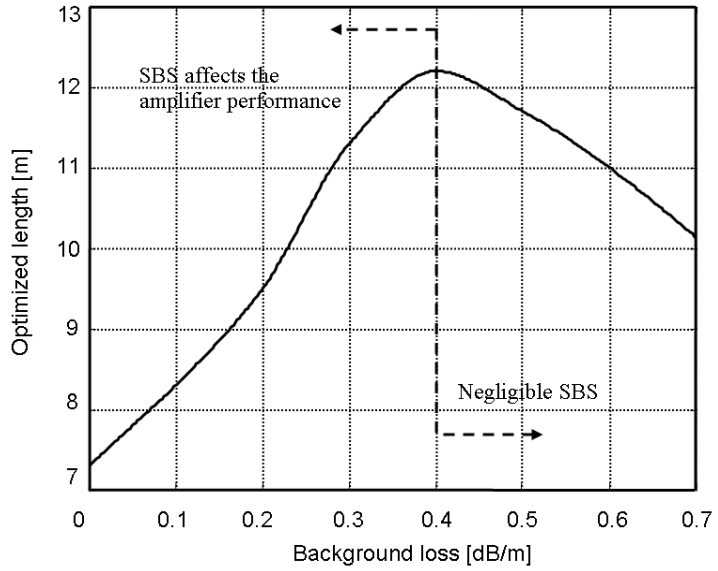

Figure 3.10: *Optimized length as a function of the background loss. The length was optimized to achieve maximum output power out of 390 W of pump power.*

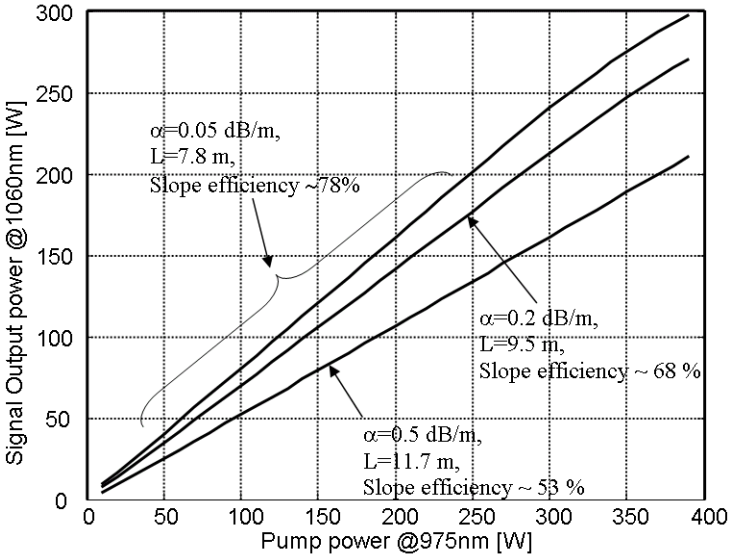

Figure 3.11: *Signal output power as a function of the pump power for different background loss values. The length of the fibres was optimized for maximum output power for a pump power equal to 390 W.*

Regarding the amplifier efficiency, the higher the background loss the smaller the output signal power for the same pump power, i.e. high background loss yields low amplifier efficiency. Figure 3.11 shows this phenomenon. The curve for the smallest value of background loss (α=0.05 dB/m) has a linear region at low pump power that

shows the highest slope efficiency; however, above 300 W pump power, the curve starts to bend because the SBS threshold has been reached. On the other hand, the curve for the fibre with the highest value of background loss (α=0.5 dB/m) is linear all over the range of pump powers shown because SBS is negligible; however, the slope efficiency for this fibre is very poor, only 53%.

3.5.3 Dependence of SBS on the fibre core radius

Regarding the effect of the core radius, it is expected that the fibre with a larger effective core area will have a higher SBS threshold because of the reduced power density in the core. This is also clear from equations (3.2) – (3.5), where it can be seen that the SBS gain is inversely proportional to the effective core area. As shown in Figure 3.12, the SBS threshold for the fibre with a smaller core radius is lower than that for fibres with a larger core radius. The inset in Figure 3.12 shows the increase of the SBS threshold as a function of the core radius. Notice that the SBS threshold is proportional to the effective mode area as happens with passive fibres [21].

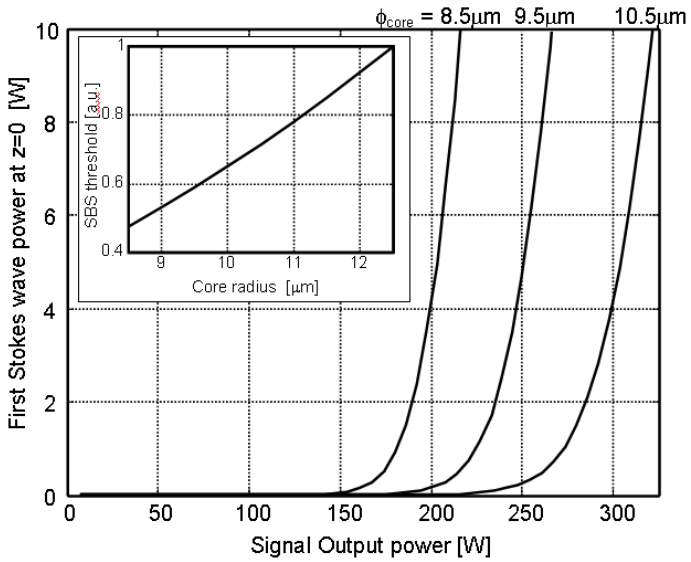

Figure 3.12: *First order Stokes power at the beginning of the fibre (z=0) as a function of the signal output power for different core radii. The trend that the SBS threshold has as a function of the core radius is shown in the inset.*

3.6 Conclusions

A model that accounts for the temperature distribution along the length in a double-clad fibre amplifier is presented. The model was used for numerical simulations with a shooting method for double-sided boundary conditions problems, and showed a good agreement with the experimental results obtained from a single-frequency, single-polarization ytterbium-doped high power fibre amplifier. The simulations confirmed that the Brillouin frequency as well as the Brillouin linewidth change in the presence of a temperature distribution along the amplifier length, and thus the effective Brillouin-gain coefficient is significantly reduced. A difference of 42 dB was observed between the Brillouin gain calculated when the fibre is considered to be at room temperature and the Brillouin gain calculated as a result of a temperature distribution proportional to the difference between the input and the output optical powers flowing through a unit of volume. The model confirmed that the output power obtained experimentally was not limited by the presence of SBS but by the available pump power.

The effect that physical characteristics of the fibre have on the amplifier SBS and thus on its performance was also presented. As expected, it was observed that high power densities in the fibre core due to small core radii and/or high pump powers, yield a low SBS threshold resulting in amplifier output powers that are limited by the amount of SBS.

A strong relationship between the fibre background loss and the fibre length was expected due to the dependence of the pump power absorption on the loss and on the interaction length. The simulations show two regions when plotting optimum amplifier length (one of these yields higher output power at a fixed pump power) as a function of the loss in the fibre. The first region is where SBS takes place and thus short fibres are required for small loss values. In the second region SBS is negligible due to the high background loss and thus longer amplifiers can be achieved. However, the efficiency of the amplifier can be affected too; therefore, the balance between power, loss and fibre length has to be carefully worked out for the desired output power.

All in all, the model presented in this work is worth considering when designing fibre amplifiers.

Bibliography

[1] M.F. dos Santos Ferreira, “Impact of Stimulated Brillouin Scattering in Optical Fibers with Distributed Gain,” J. Lightwave Technol. 13(8), 1692-1697 (1995).

[2] N.A. Brilliant, “Stimulated Brillouin scattering in a dual-clad fiber amplifier,” J. Opt. Soc. Am. B 19(11), 2551-2557 (2002).

[3] Y. Jeong, J. Nilsson, J.K. Sahu, D.B.S. Soh, C.A. Alegria, P. Dupriez, C.A. Codemard, D.N. Payne, R. Horley, L.M.B. Hickey, L. Wanzcyk, C. Chryssou, J.A. Alvarez-Chavez, P.W. Turner, “Single-frequency, single-mode, single-polarization ytterbium-doped fiber MOPA source with 264 W of continuous-wave output power,” in OSA Trends in Optics and Photnics Series (TOPS) Vol. 96, Conference on Lasers and Electro-Optics (CLEO), Technical Digest, Postconference Edition (Optical Society of America, Washington, DC 2004), paper CPDD1 (2004).

[4] C.N. Pannell, P. St. J. Russell, T. Newson, “Stimulated Brillouin Scattering in Optical Fibers: the Effects of Optical Amplification,” J. Opt. Soc. Am. B 10(4), 684-690 (1993).

[5] S.L. Zhang, J.J. O'Reilly, “Effect of Stimulated Brillouin Scattering on Distributed Erbium-Doped Fiber Amplifier,” IEEE Photon. Technol. Lett. 5(5), 537-539 (1993).

[6] R. Paschotta, J. Nilsson, A.C. Tropper, D.C. Hanna, “Ytterbium-Doped Fiber Amplifiers,” IEEE J. of Quantum Electron. 33(7), 1049-1056 (1997).

[7] C.C. Renaud, High Power Diode-Pumped Ytterbium-Doped Fibre Lasers, PhD Thesis (University of Southampton, Southampton, UK, 2003).

[8] S. Le Flohic, P. Cambon, "Study of Brillouin gain spectrum in standard single-mode optical fiber at low temperatures (1.4-370 K) and high hydrostatic pressures (1-250 bars)," Opt. Comm. 219, 395-410 (2003).

[9] J. Hansryd, F. Dross, M. Westlund, P.A. Andrekson, S.N. Knudsen, "Increase of the SBS Threshold in a Short Highly Nonlinear Fiber by Applying a Temperature Distribution," J. Lightwave Technol. 19(11), 1691-1697 (2001).

[10] T. Kurashima, T. Horiguchi, M. Tateda, "Thermal Effects of Brillouin Gain Spectra in Single-Mode Fibers," IEEE Photon. Technol. Lett. 2(10), 718-720 (1990).

[11] Q. Yu, X. Bao, L. Chen, "Temperature dependence of Brillouin frequency, power, and bandwidth in panda, bow-tie, and tiger polarization-maintaining fibers," Opt. Lett. 29(1), 17-19 (2004).

[12] Y. Imai, N. Shimada, "Dependence of Stimulated Brillouin Scattering on Temperature Distribution in Polarization-Maintaining Fibers," IEEE Photon. Technol. Lett. 5(11), 1335-1337 (1993).

[13] M. Nikles, L. Thevenaz, P.A. Robert, "Brillouin Gain Spectrum Characterization in Single-Mode Optical Fibers," J. Lightwave Technol. 15(10), 1842-1851 (1997).

[14] Y. Wang, "Heat Dissipation in Kilowatt Fiber Power Amplifiers," IEEE J. Quantum Electron. 40(6), 731-740 (2004).

[15] Y. Wang, C.Q. Xu, H. Po, "Thermal Effects in Kilowatt Fiber Lasers," IEEE Photon. Technol. Lett. 16(1), 63-65 (2004).

[16] J.W. Yu, Y. Park, K. Oh, I.B. Kwon, "Brillouin frequency shifts in silica optical fiber with the double cladding structure," Opt. Exp. 10(19), 996-1002 (2002).

[17] N. Shibata, R.G. Waarts, R.P. Braum, "Brillouin-gain spectra for single-mode fibers having pure-silica, GeO2-doped, and P2O5-doped cores," Opt. Lett. 12(4), 269-271 (1987).

[18] M. Ohashi, M. Tateda, "Design of Strain-Free-Fiber with Nonuniform Dopant Concentration for Stimulated Brillouin Scattering Suppression," J. Lightwave Technol. 11(12), 1941-1945 (1993).

[19] N. Yoshizawa, T. Imai, "Stimulated Brillouin Scattering Suppression by Means of Applying Strain Distribution to Fiber with Cabling," J. Lightwave Technol. 11(10), 1518-1522 (1993).

[20] N. Yoshizawa, T. Horiguchi, T. Kurashima, "Proposal for Stimulated Brillouin Scattering Suppression by Fibre Cabling," Electron. Lett. 27(12), 1100-1101 (1991).

[21] Agrawal, G.P., Nonlinear Fiber Optics, 3rd ed. (Academic Press, San Diego, CA, 2001).

Chapter 4

4 Distributed Brillouin Gain Spectrum Measurements

4.1 Introduction

Fibre amplifiers have to be designed with the non-linear phenomena that may appear at the desired output power in mind. In the case of narrow-linewidth fibre lasers and amplifiers, stimulated Brillouin scattering has to be considered even before the fibre structure and doping characteristics are decided. The model presented in chapter 3 is very useful when designing fibre amplifiers since the effect of the fibre geometry and composition on the amplifier performance can be obtained. However, in order to produce results closer to reality, the model requires input values of actual Brillouin scattering characteristics for the fibre such as the Brillouin gain or the Brillouin frequency shift. This chapter presents a measuring technique to obtain the Brillouin gain spectrum of fibres with different dopants and structures.

4.2 Measurement system

The measurement technique was a microwave detection system for coherent detection of the anti-Stokes spontaneous Brillouin backscatter developed by Dr.

Mohammed Nasser Al Ahbabi from the Distributed Optical Fibre Sensors Group at the ORC [1][2]. The set up is shown in Figure 4.1.

The laser source is a tuneable laser at 1533.2 nm, with ~1MHz linewidth. The beam passes through an Erbium-doped Amplifier (EDFA) and an Acousto Optic Modulator (AOM) to generate a pulse. The width of the generated pulse will determine the spatial resolution of the system. In addition, the source beam is used as an Optical Local Oscillator (LO) for coherent detection of the anti-Stokes Brillouin signal [1][3]. In order to achieve a shorter pulse that yielded better spatial resolution, the AOM was replaced by an Electro Optic Modulator (EOM).

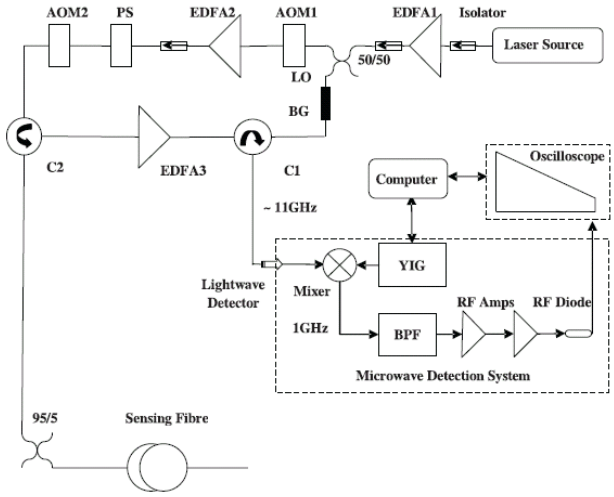

Figure 4.1: *Experimental arrangement for measuring Brillouin frequency shift using a microwave detection system. EDFA: erbium-doped fibre amplifier; AOM: acousto-optic modulator; PS: polarization scrambler; LO: local oscillator; BG: Bragg grating; C: circulator; LD: lightwave detector; YIG: YIG synthesizer; BPF: band-pass filter. After [1].*

The pulse will travel through the fibre under test (FUT) and will generate a backscattered signal (mainly Brillouin and Rayleigh) which in turn will be amplified by the third EDFA (EDFA3). The amplified backscattered signal will go through the fibre Bragg grating (BG) to combine with the LO. The Bragg grating allows the intermediate frequency signal resulting from the combination of the anti-Stokes Brillouin signal and the LO to go back into the system. The intermediate frequency will be approximately equal to the Brillouin shift. This signal mixes with a PC controlled YIG-based Electrical Local Oscillator (ELO) and is passed through a 1 GHz Band Pass Filter (BPF) which in turn will generate a 1 GHz intermediate

frequency with 50 MHz bandwidth. The ELO is scanned through a wide range of frequencies in defined steps, each of those frequencies determines the Brillouin beat frequency measured. The measured component of the BGS is equal to the ELO frequency plus the 1 GHz intermediate frequency minus the frequency shift induced by the EOM that generated the pulse. After the BPF, the signal is amplified and rectified generating a signal proportional to the intensity of the backscattered signal at each particular frequency. The Oscilloscope is used to average the time-domain traces from along the fibre and the amplitude, frequency and position information is transferred to a PC where a three dimensional image of the BGS can be built.

4.3 Structure and Composition of the Measured Fibres

The measurements presented here are from fibres fabricated at the ORC using the MCVD solution doping technique. The composition and structure of the fibres selected for characterisation are summarised in Table 4.1.

Table 4.1: *Characterised fibre properties.*

Fibre	Dopants	Structure	Diameter [µm]	Length [m]	Loss at 1533 nm [dB/m]	N.A.
A	Al	Non-tapered single core. Additional Cl2 dehydration to obtain low OH	125	300	0.010	0.1
B	5g Al	Non-tapered single core	130	100	0.138	0.12
C	10g Al	Non-tapered single core	105	244	0.143	0.14
D	Ge/Yb	Non-tapered single core central dip	96	150	0.036	0.13
E	Al/Ge	Outer core: Ge (tapered) Inner core: Al (uniform)	100	100	0.180	0.12

The fibre structures shown in Table 4.1 are schematically depicted in Figure 4.2. Figure 4.2(a) shows a uniform core/cladding structure, here the core is uniformly doped along the fibre and its diameter remains constant also through the length of the fibre. Finally, Figure 4.2(b) shows a tapered configuration in a double core structure. In this structure, the outer core diameter varies with the fibre length while the inner core remains uniform in size along the fibre.

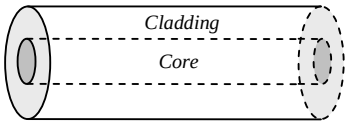

(a) Non-tapered single core/cladding structure

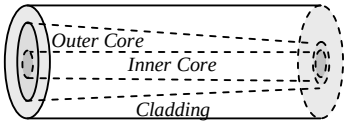

(b) Tapered dual-core structure

Figure 4.2: *Structures used in the fibres measured.*

In order to have a reference, in all cases the fibre under test was spliced at both ends to a single mode fibre (SMF). The reference fibre was a conventional SMF used for telecommunications, it had a loss of 0.20 dB/km, a core of 6 µm, an outer diameter of 125 µm, and an effective area of 80 μm^2.

Figure 4.3 shows the measured BGS for the single mode fibre used as reference. The measured linewidth and Brillouin frequency are in good agreement with the textbook values of 36 MHz and 11 GHz respectively [4]. The data from each spectra was fitted to a Lorentzian function to measure the linewidth and frequency shift. The linewidth shown is the full width at half maximum (FWHM) of the amplitude observed, this was the standard used to calculate the linewidths of the other fibres measured.

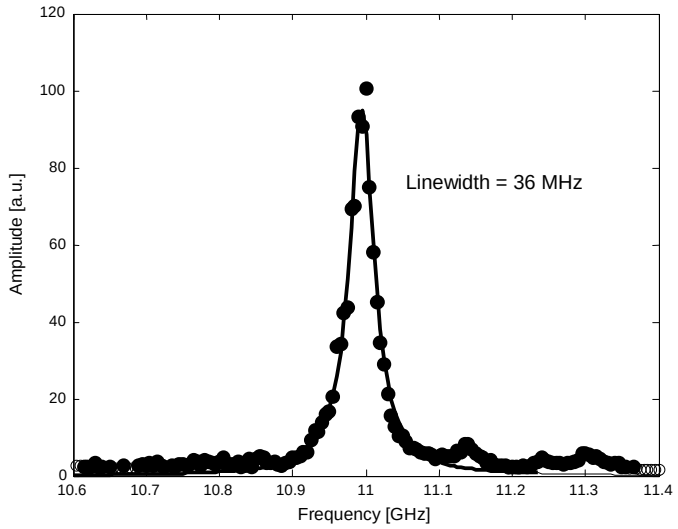

Figure 4.3: *Brillouin Gain Spectrum for the single mode fibre used for reference.*

4.4 Experimental Results

Figure 4.4(a) shows the BGS as a function of the fibre length and Figure 4.4(b) the BGS at the beginning of fibre *A*.

This is a non-tapered fibre with an aluminum (Al) doping. This fibre exhibits two peaks for the Brillouin gain very close to each other and hence, for simplicity, they are being considered as one main peak with $\nu_B \approx 11.37$ GHz.

As expected, this fibre presents a much larger linewidth (270 MHz) compared to that exhibited by the reference SMF (36 MHz).

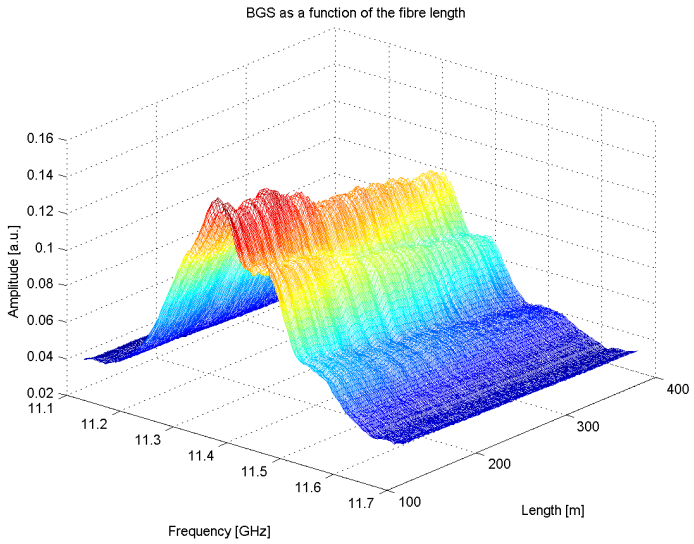

(a) Brillouin Gain Spectrum along fibre A.

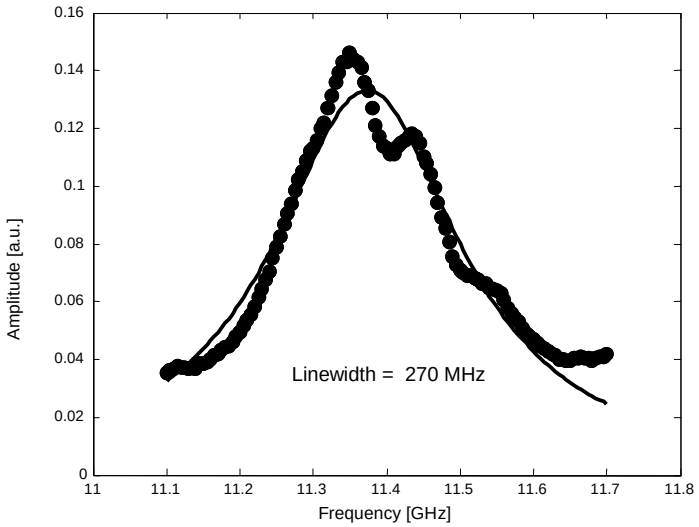

(b) Brillouin Gain Spectrum at the beginning of fibre A.

Figure 4.4: *Measured Brillouin Gain Spectrum from fibre A.*

Figure 4.5(a) shows the BGS as a function of the fibre length and Figure 4.5(b) the BGS at the beginning of fibre *B.*

This fibre is similar to fibre *A* in the sense that it is also Aluminum doped. However, the doping concentration is higher resulting also in a higher background loss. The linewidth for this fiber was around 240 MHz. This fibre also exhibits two adjacent

peaks for the Brillouin gain. Again, for simplicity, they are being considered as one main peak with $\nu_B \approx 11.36$ GHz, which is almost the same as in fibre *A*.

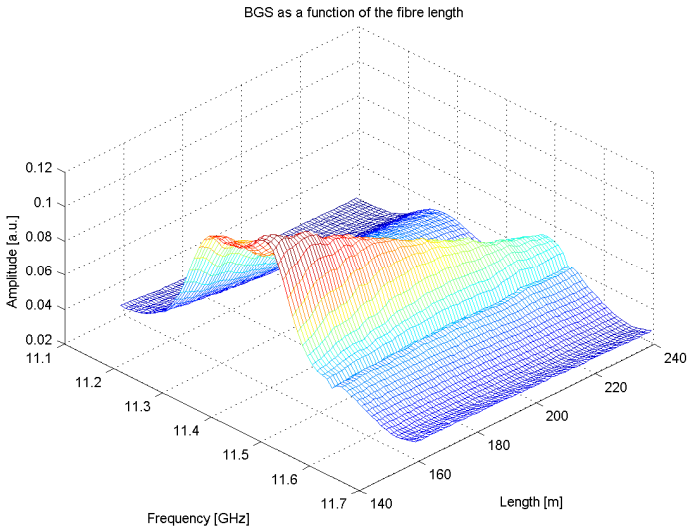

(a) Brillouin Gain Spectrum along fibre B.

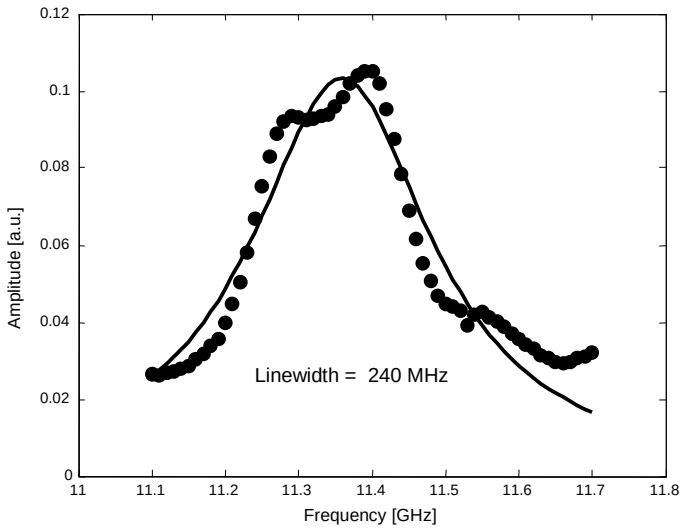

(b) Brillouin Gain Spectrum at the beginning of fibre B.

Figure 4.5: *Measured Brillouin Gain Spectrum from fibre B.*

Fiber *C* has a very similar structure to fibre *B* but with an even higher doping concentration. Figure 4.6(a) shows the BGS as a function of the fibre length and Figure 4.6(b) the BGS at the beginning of the fibre for fibre *C*. This fibre is similar to fibre *B* in structure and dopant, however, the doping solution contained twice the

concentration of aluminum compared to the one used to make fibre *B*, resulting in a higher background loss. The linewidth for this fibre was around 200 MHz. This fibre only exhibits one main peak for the Brillouin gain at $\nu_B \approx 11.6$ GHz. This is around 230 MHz above the frequency of the one present in fibres *A* and *B* which suggests that the doping concentration may have an effect on the density of the material and thus on the acoustic wave velocity and on the frequency shift of the Brillouin scattering.

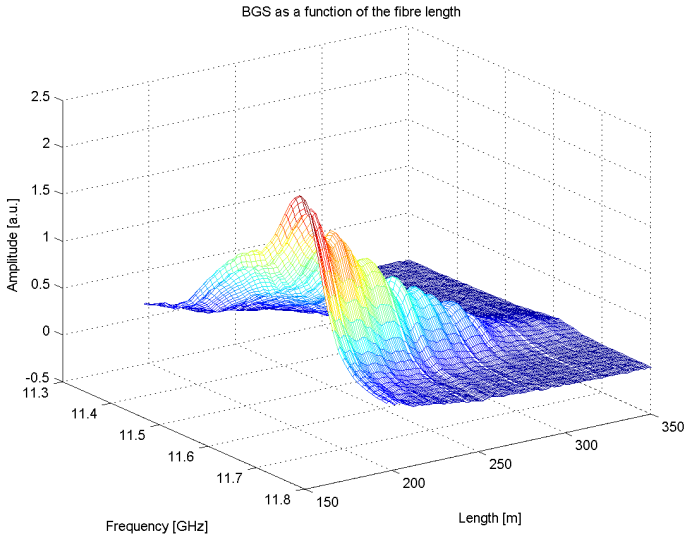

(a) Brillouin Gain Spectrum along fibre C.

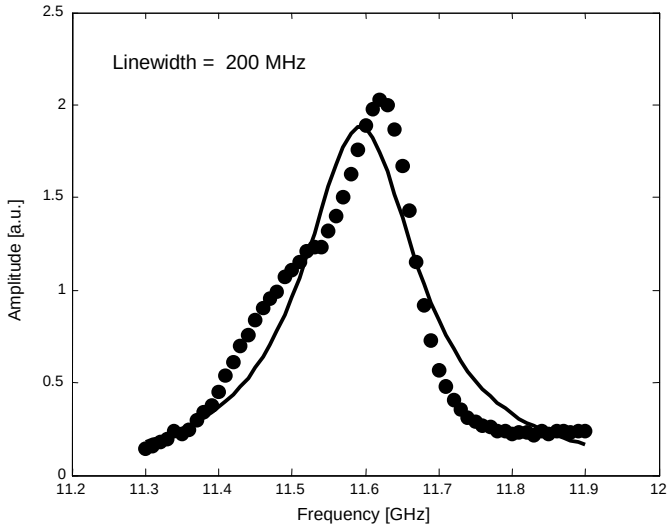

(b) Brillouin Gain Spectrum at the beginning of fibre C.

Figure 4.6: *Measured Brillouin Gain Spectrum from fibre C.*

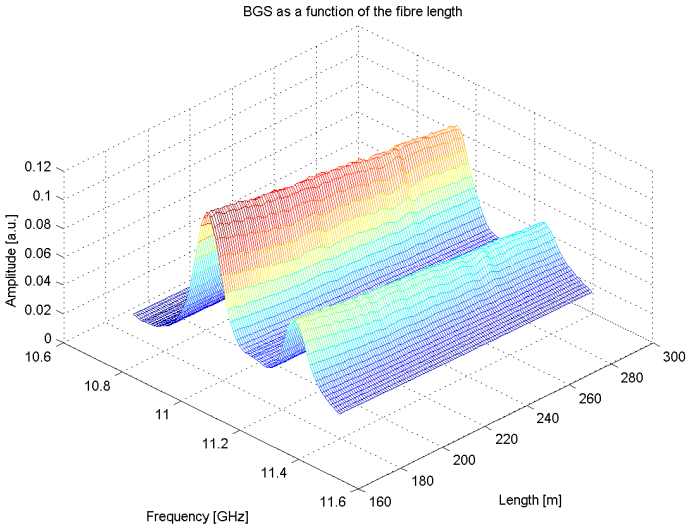

(a) Brillouin Gain Spectrum along fibre D.

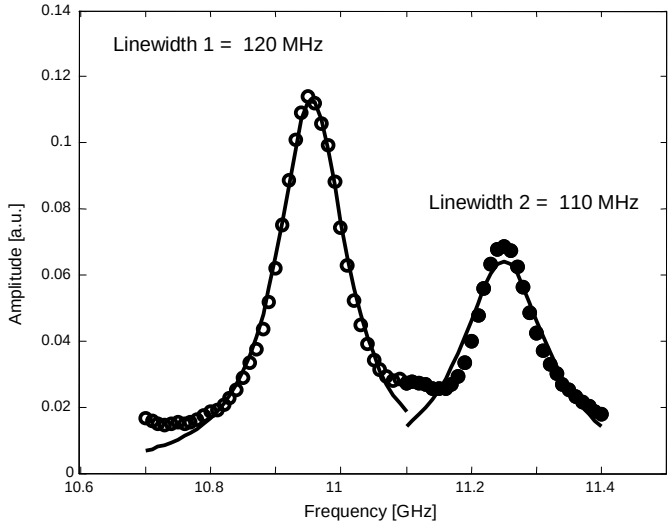

(b) Brillouin Gain Spectrum at the beginning of fibre D.

Figure 4.7: *Measured Brillouin Gain Spectrum from fibre D.*

Figure 4.7 presents the BGS for a single core fibre with a huge central dip in the refractive index profile. The refractive index profile for the preform of this fibre is shown in Figure 4.8. The dopants for this fibre are germanium and ytterbium. In this case, two main peaks can be observed for the Brillouin gain. The biggest peak is close to the one present in the SMF, it is located approximately at 10.96 GHz. The

second peak is situated at ~11.25 GHz. The second peak could be a contribution of Yb in silica; however, further study is required to confirm it. The linewidth for the first peak is ~120 MHz, while for the second peak it is around 110 MHz. It is quite likely that due to the dip in the refractive index profile the linewidth of the first peak in Figure 4.7 gets broader (~120 MHz) than the SMF fibre (~ 36 MHz).

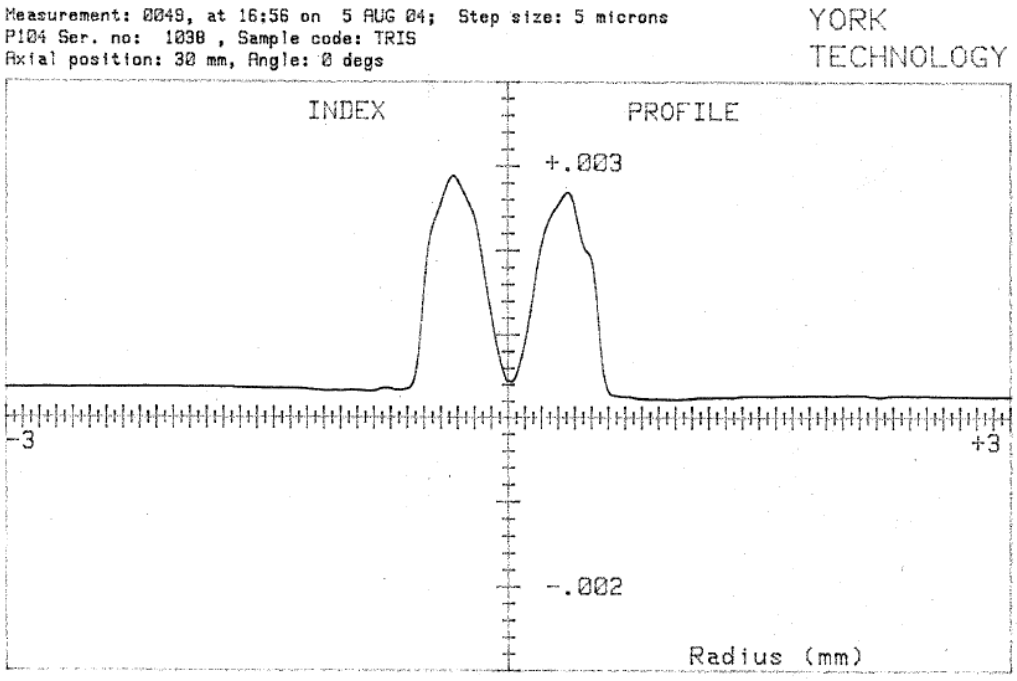

Figure 4.8: *Refractive index profile of the preform used for fibre D.*

Finally, Figure 4.9 shows the BGS for fibre *E*. Fibre *E* is also a double core fibre but this time the inner core is tapered. This fibre also presents two main peaks, one at ~11.18 GHz and the larger one at ~11.31 GHz. The linewidths for both peaks are 80 MHz and 120 MHz respectively. Since this fibre is tapered, Figure 4.9(a) shows that around 40 m into the fibre, the amplitude of the peak at ~11.31 GHz has been reduced considerably and only one very broad spectrum with central frequency at ~11.26 GHz and Brillouin linewidth of ~290 MHz remains.

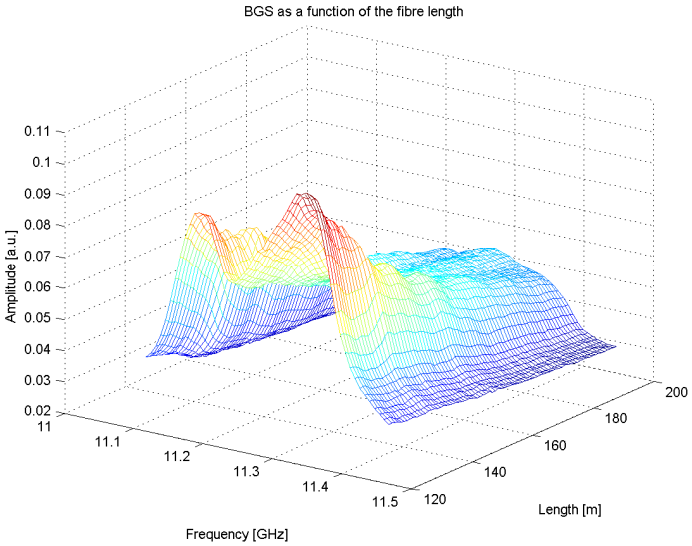

(a) Brillouin Gain Spectrum along fibre E.

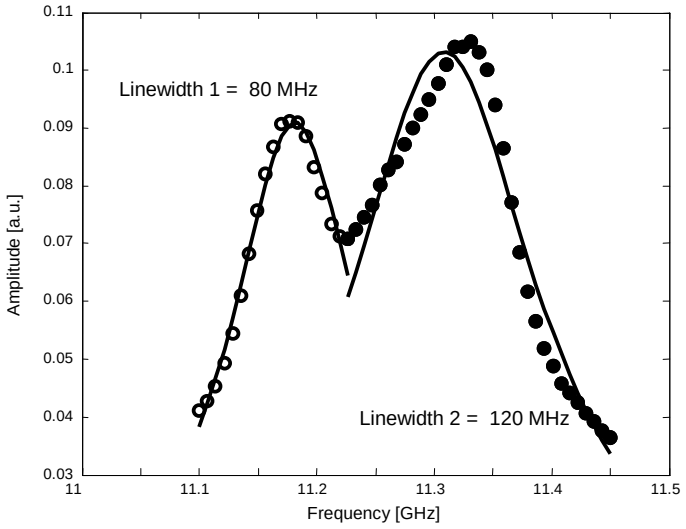

(b) Brillouin Gain Spectrum at the beginning of the fibre for fibre E.

Figure 4.9: *Measured Brillouin Gain Spectrum from fibre E.*

Table 4.2 summarises the structure, dopants and Brillouin characteristics measured in the fibres under test.

Table 4.2: *Brillouin frequency shift and linewidth of the fibres under test..*

Fibre	Dopants	Structure	Brillouin frequency shift [GHz]	Linewidth [MHz]
A	Al	Non-tapered single core	11.37	270
B	5g Al	Non-tapered single core	11.36	240
C	10g Al	Non-tapered single core	11.59	200
D	Ge/Yb	Non-tapered single core central dip	10.96 / 11.25 2 peaks	120 / 110 2 peaks
E	Al/Ge	Outer core: Ge (tapered) Inner core: Al (uniform)	11.18 / 11.31 2 peaks	80 / 120 2 peaks

Fibres *A* and *B* present very similar characteristics since both are single core fibres with aluminum as co-dopant. However, fiber *C* is also co-doped with Al and presents a narrower linewidth and a larger frequency shift. This is due to the large doping concentration of Al in fibre *C*. Higher dopant concentrations change the density of the fibre resulting in different acoustic properties and hence the frequency shift will be different.

Fibres *A*, *B*, and *C* were only doped with Al and thus the presence of multiple peaks shouldn't be justified as with fibres *D* and *E* that have two different dopants. However, these fibres also exhibit two distinct peaks, though they are spaced closer together in these cases. Since the fibres are large area mode fibres, several acoustic propagation modes that travel at different velocities may appear and produce broad multipeak Brillouin spectra. However, because of the presence of a single dopant, the propagation velocities of the acoustic modes are close resulting in peaks also

close to each other. Therefore the fitting to individual peaks becomes unfeasible, hence, in these cases it was decided to consider the spectrum as a single broad one and to fit them to a simple Lorentzian curve in order to obtain their characteristics.

In fibre *E*, the dopants in the core and inner cladding (or secondary core) are different, thus the acoustic modes in each layer are different resulting in the two peaks observed; furthermore, because of the fibre tapered structure, the BGS in this fibre gets broader with the position along the fibre and the peaks merge into a single one. Regarding fibre *D*, the dual peak spectrum may be attributed to the presence of two dopants, Yb and Ge; however, this requires further study to confirm it.

4.5 Conclusions

Brillouin Gain Spectrum measurements were obtained by means of a microwave detection system for the coherent detection of the anti-Stokes spontaneous Brillouin backscatter. The fibres tested were fabricated at the ORC with different physical characteristics as well as dopants and doping concentrations.

It was observed that the structure and doping concentration have a big impact on the Brillouin scattering characteristics such as the Brillouin frequency shift and the Brillouin linewidth. It was shown that different dopants induce different acoustic modes resulting in shifts associated to the kind of dopant and its concentration.

Regarding fibre structure, the fibre with dual core constitution presented two distinctive Brillouin peaks. The reason behind this is that each core is doped differently and thus each layer has a different acoustic mode; therefore, two backscattered waves with a different frequency shift arise. In the amplifier, this will produce two different backscattered signals at different frequencies. On the other hand, it was shown that a tapered secondary core structure presents a BGS that changes with the position along the fibre. It was demonstrated that this kind of structure helps broadening the Brillouin gain spectrum and thus reducing the effective Brillouin gain.

The wide broadening of the Brillouin gain spectrum observed in all cases mainly obeys to the heavy doping in the fibres. It is well documented that a short damping time of the acoustic waves leads to a broader spectrum [4], and since the doping concentration and kind of dopant have a big effect on the acoustic nature of the fibres, it can be concluded that the high amount of dopant in these fibres reduce the effective phonon lifetime resulting in the broadening of the spectrum. Moreover, inhomogeneities in the core-cladding interface and concentration variation along the fibres also contribute to the Brillouin spectrum broadening.

Bibliography

[1] M.N. Alahbabi, N.P. Lawrence, Y.T. Cho, T.P. Newson, "High spatial resolution microwave detection system for Brillouin-based distributed temperature and strain sensors," Meas. Sci. Technol. **15**(8), 1539-1543 (2004).

[2] M.N. Al Ahbabi, Distributed Optical Fibre Sensors Based on the Coherent Detection of Spontaneous Brillouin Scattering, PhD Thesis (University of Southampton, Southampton, UK, 2005).

[3] M.N. Alahbabi, Y.T. Cho, T.P. Newson, "100 km distributed temperature sensor based on coherent detection of spontaneous Brillouin backscatter," Meas. Sci. Technol. 15(8), 1544-1547 (2004).

[4] Agrawal, G.P., Nonlinear Fiber Optics, 3rd ed. (Academic Press, San Diego, CA, 2001).

Chapter 5

5 Conclusions

5.1 Summary and Conclusions

This thesis has presented theoretical and experimental research on how to minimize the amount of stimulated Brillouin scattering in high power fibre lasers and amplifiers. The research focuses on the effect a temperature distribution along the fibre and the fibre structure and fibre doping characteristics have on the SBS threshold.

A mathematical model for the pump, seed, and multiple order Stokes waves in a narrow-line single frequency double-clad fibre amplifier was implemented using MATLAB®. The model was used to identify the key parameters of the fibre structure that affect the SBS threshold. The effect that the fibre length, core size, and doping concentration have on the amount of SBS and on the amplifier output power was quantified. It was shown that efficient fibre amplifiers with an output power limited by the available pump power and not by the amount of SBS can be achieved by optimizing the pump absorption length through the manipulation of the fibre length and doping concentration. Furthermore, the model verified that a high doping concentration can limit the presence of SBS and the length can be adjusted accordingly to produce 'SBS free' output powers. The numerical simulations showed that above a certain value of background loss, the SBS does not affect the amplifier performance at all, and the optimum length of the amplifier decreases as

the background loss increases. Conversely, for low values of background loss, the SBS gain takes over the amplifier's gain. As a result, the length optimization process in an amplifier tends to make the fibre shorter as the background loss is reduced. This happens in order to shrink the effective nonlinear interaction length; in turn, the Brillouin gain is also reduced and the output power is maximized.

It was also confirmed that large area mode fibres will show a higher SBS threshold due to the smaller power densities present in the amplifier.

To the author's knowledge, for the first time a model was implemented to account for the effect a temperature distribution along the fibre has on the amplifier performance and on the amount of SBS generated when high power outputs are desired. The results of the simulations proved to be in close agreement with experimental results previously reported of a single-frequency, single-polarization ytterbium-doped dual-clad high power fibre amplifier. The model verified that the temperature distribution along the fibre was the reason behind the high power achieved through experimentation even when it was thought that SBS would limit the output power of the amplifier. Through simulations, it was demonstrated that the frequency shift, the Brillouin linewidth and the peak Brillouin gain, are extremely affected by the temperature distribution. Using the parameters from the referenced experiment, the simulations showed a difference of 42 dB between the Brillouin gain calculated when the fibre is considered to be at room temperature, and the Brillouin gain calculated as a result of a temperature distribution proportional to the difference between the input and the output optical powers. Furthermore, the model showed that the Brillouin linewidth increases more than twice when the temperature change is considered. Therefore, it is of utmost importance to take into consideration the effects of a temperature distribution along the fibre when calculating the SBS threshold in high power fibre devices.

All in all, the model proved to be reliable and helpful when designing the fibre for the final amplification stage of high power fibre amplifiers and lasers.

Measurements to determine the Brillouin frequency and Brillouin linewidth in fibres with different geometries and compositions were performed using a microwave detection system for coherent detection of the anti-Stokes spontaneous Brillouin backscatter. The measurement system was implemented by the Distributed Optical Fibre Sensors Group at the ORC. The set-up was developed to enable the

measurement on high background loss fibres. The results obtained showed that the Brillouin linewidth and Brillouin frequency are very much dependent on the fibre's geometry and composition. For instance, a dual peak Brillouin gain spectrum was observed when a fibre with a dual-core structure was measured. It was also observed that the kind of dopant and its concentration affect the acoustic modes in the fibre thus resulting in broad linewidths and different frequency shifts.

In general, it can be concluded that the model implemented here, in combination with Brillouin gain spectrum measurements, can have a significant impact when trying to suppress the stimulated Brillouin scattering in high power fibre lasers and amplifiers. Modelling of the waves in the amplifier affected by an estimated temperature distribution can be used to manipulate the fibre structure and composition in order to achieve a high SBS threshold.

5.2 Future Work

Further modelling has to be performed in order to achieve a broader understanding of the effect that the fibre's geometry has on the SBS threshold. The next step would be to study the effect a tapered core has on the backscattered power.

The model can be improved to account for other key parameters that increase the SBS threshold. Regarding the temperature effect on the SBS, the change on the radial temperature in the fibre can also be included. In addition, the strain in the fibre should also be modelled.

Moreover, different index profiles should be implemented in the model to study its effect on the Brillouin scattering present in the amplifier.

In relation to the doping concentration, since the higher the doping concentration the shorter the amplifier length and in turn the higher the SBS threshold, it can be pushed up to the point before rare-earth clustering appears. The damage threshold in a high Yb-doped fibre must be studied. In other words, research on the correlation between the damage threshold and the doping concentration must be carried out.

Appendix A

A. List of Publications

D.N. Payne, Y. Jeong, J. Nilsson, J.K. Sahu, D.B.S. Soh, C. Alegria, P. Dupriez, C.A. Codemard, V.N. Philippov, V. Hernandez, R. Horley, L. Hickey, L. Wanzcyk, C.E. Chryssou, J.A. Alvarez-Chavez, P.W. Turner, "Kilowatt-class single-frequency fiber sources," in Proc. SPIE 5709, 133-141 (2005).

V.I. Kovalev, R.G. Harrison, J. Nilsson, Y. Jeong, V. Hernandez-Solis, J.K. Sahu, "Analytic modeling of Brillouin gain in rare-earth doped fiber amplifiers with high-power single-frequency signals," in Fiber Lasers Technology, Systems and Applications II, Proc. SPIE 5709, paper 23 (2005).